

Bæredygtigt arktisk byggeri i det 21. århundrede

Vakuumsølsfangere – Statusrapport 3 til
VILLUM KANN RASMUSSEN FONDEN

Sagsrapport
BYG·DTU SR-06-02
2006
ISSN 1601 - 8605

Bæredygtigt arktisk byggeri i det 21. århundrede

Vakuumsørfangere – Statusrapport 3 til
VILLUM KANN RASMUSSEN FONDEN

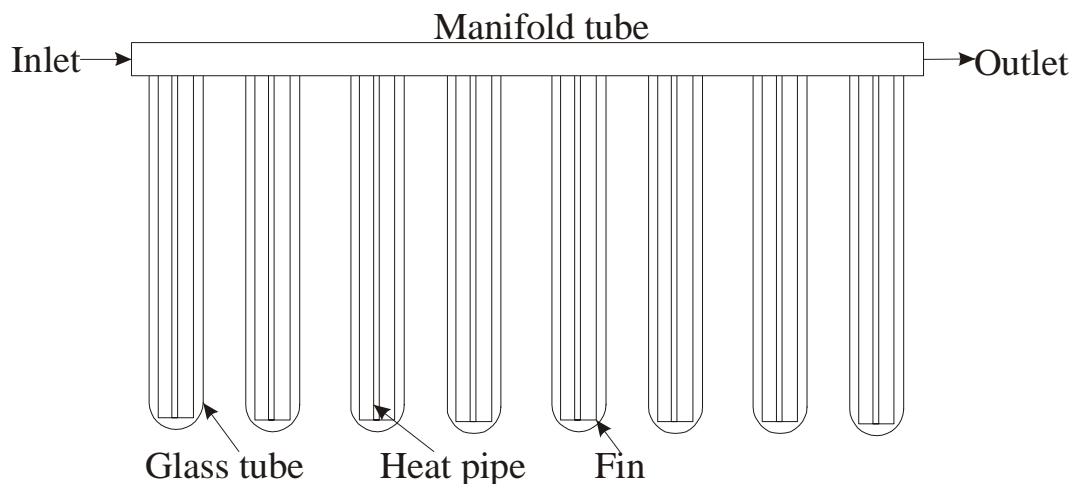
Jianhua Fan, Louise Jivan Shah, Simon Furbo

Indholdsfortegnelse

Indholdsfortegnelse	5
Forskningsindhold.....	6
Publikationer	8
Foredrag	8
Anden formidling	8
Regnskab.....	9
Bilag 1: NorthSun 2005 paper: Utilization of solar radiation at high latitudes with evacuated tubular collectors.....	10
Bilag 2: Solar World Congress 2005 paper: Theoretical investigations of differently designed heat pipe evacuated tubular collectors.....	21
Bilag 3: Solar World Congress 2005 paper: Numerical investigations of an all glass evacuated tubular collector.	28
Bilag 4: North Sun 2005 Congress præsentation: Utilization of solar radiation at high latitude with evacuated tubular collectors.	35
Bilag 5: ISES Solar World Congress præsentation: Theoretical investigations of differently designed heat pipe evacuated tubular collectors.....	48
Bilag 6: ISES Solar World Congress præsentation: Theoretical investigations of an all glass evacuated tubular collector.....	57
Bilag 7: Præsentation ved Solar seminar ved Beijing Solar Energy Institute, Beijing, Kina: Side-by-side tests of Seido collectors	64

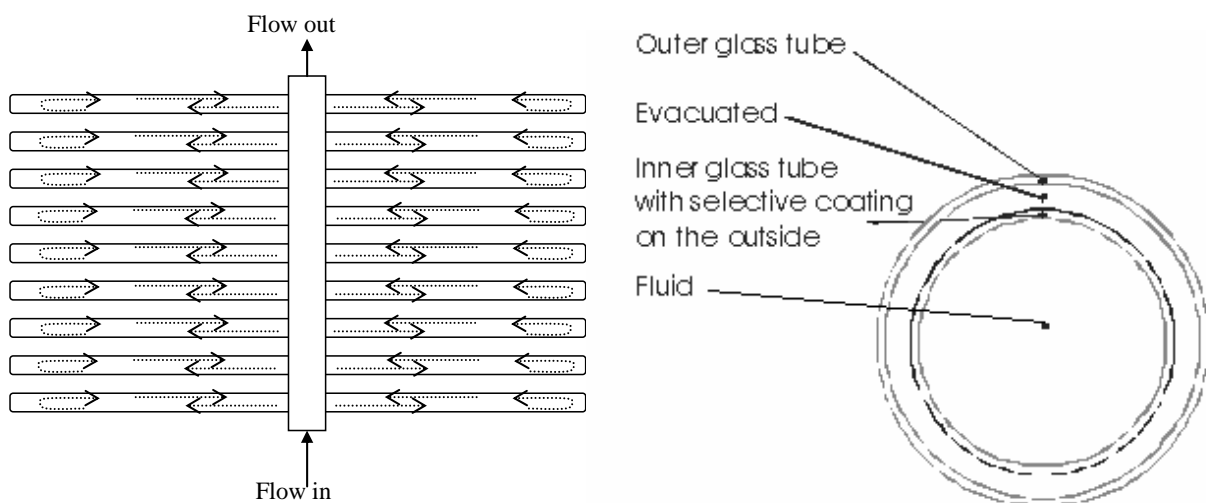
Forskningsindhold

I projektets tredje år er de udviklede detaljerede matematiske modeller for heat pipe vakuumrørsolfangere med krumme og plane finner benyttet til at beregne ydelsen af forskelligt udformede vakuumrørsolfangere i Uummannaq i Grønland, i Sisimiut i Grønland og i København, se figur 1.



Figur 1. Principskitse af heat pipe vakuumrørsolfanger.

Der er desuden gennemført detaljerede teoretiske undersøgelser af en all glass vakuumrørsolfanger, hvor solfangervæsken opvarmes ved direkte kontakt med de indvendige solopvarmede glas, se figur 2. Undersøgelserne, som er gennemført ved hjælp af CFD (Computational Fluid Dynamics) beregninger, har klarlagt, hvorledes flowfordelingen i solfangeren og solfangereffektiviteten afhænger af volumenstrømmen gennem solfangeren.



Figur 2. Principskitse af all glass vakuumrørsolfanger med solfangervæsken direkte placeret i det indvendige glastrør.

Prøvestanden for vakuumrørsolfangere, der udnytter solstråling fra alle retninger, er blevet færdigopbygget. I prøvestanden er der gennemført målinger af ydelser af 5 forskelligt udformede vakuumrørsolfangere under ens driftsbetingelser, se figur 3. Alle solfangerne er produceret af kinesiske fabrikker. Ydelserne er målt i perioder med forskellige driftstemperaturer.



Figur 3. 5 vakuumrørsolfangere under afprøvning i prøvestand.

I sidste del af projektet vil målingerne i prøvestanden blive videreført og målingerne vil blive benyttet til at validere de udviklede simuleringsmodeller for vakuumrørsolfangere baseret på heat pipe princippet. Derefter vil der blive gennemført beregninger med de validerede modeller for at bestemme årlige ydelser for forskelligt udformede vakuumrørsolfangere. Baseret på disse beregninger og på priser for solfangerne vil egnetheden af de forskellige solfangere til arktiske solvarmeanlæg blive bestemt.

Publikationer

- Shah L.J., Furbo S. (2005) *UTILIZATION OF SOLAR RADIATION AT HIGH LATITUDES WITH EVACUATED TUBULAR COLLECTORS*. North Sun 2005 Congress, Vilnius, Lithuania.
- Shah L.J., Furbo S. (2005) *THEORETICAL INVESTIGATIONS OF DIFFERENTLY DESIGNED HEAT PIPE EVACUATED TUBULAR COLLECTORS*. ISES Solar World Congress, 2005, Orlando
- Shah L.J., Furbo S. (2005) *NUMERICAL INVESTIGATIONS OF AN ALL GLASS EVACUATED TUBULAR COLLECTOR*. ISES Solar World Congress, 2005, Orlando

Foredrag

- Shah L.J. (2005) *Utilization of solar radiation at high latitudes with evacuated tubular collectors*. North Sun 2005 Congress, oral presentation, May 25-27, 2005.
- Shah L.J. (2005) *Numerical Investigations of an All Glass Evacuated Tubular Collector*. ISES Solar World Congress, oral presentation, Orlando, August 07-12 2005.
- Shah L.J. (2005) *Theoretical Investigations of differently designed Heat Pipe Evacuated Tubular Collectors*. ISES Solar World Congress, oral presentation, Orlando, August 07-12 2005.
- Shah L.J. (2005) *Side-by-side tests of Seido collectors*. Solar Seminar, Beijing Solar Energy Institute, Beijing, China, October 27, 2005.

Anden formidling

Der er ydet vejledning til to DTU studerende, som i efteråret 2005 gennemførte midtvejsprojekt vedrørende vakuumrørsolfangere til Arktis. De studerende analyserede blandt andet målinger for de vakuumrørsolfangere, som afprøves i prøvestanden.

Regnskab

Indbetalinger	<u>2,241,000.00</u>
---------------	---------------------

Indtægter i alt	2,241,000.00
------------------------	---------------------

Forskertimer	1,226,461.77
--------------	--------------

Teknisk/adm. bistand	274,874.63
----------------------	------------

Rejser	49,153.53
--------	-----------

Drift og materialer	141,672.26
---------------------	------------

Øvrige	9,093.03
--------	----------

Udgifter i alt	1,701,255.22
-----------------------	---------------------

Saldo projektkonto	539,744.78
---------------------------	-------------------

Bilag 1: NorthSun 2005 paper: Utilization of solar radiation at high latitudes with evacuated tubular collectors

UTILIZATION OF SOLAR RADIATION AT HIGH LATITUDES WITH EVACUATED TUBULAR COLLECTORS

Louise Jivan Shah and Simon Furbo

Department of Civil Engineering, Technical University of Denmark, Building 118, DK-2800 Kgs. Lyngby, Denmark
Phone: +45 45 25 18 88, Fax: +45 45 93 17 55, E-mail: ljs@byg.dtu.dk

Abstract – Theoretical investigations of how two differently designed ground mounted heat pipe evacuated tubular collectors utilize the solar radiation at high latitudes have been carried out. The absorber fins in the evacuated tubes are either flat or curved and the fins have selective coating on both sides so that solar radiation from all directions can be utilized. The yearly thermal performance of heat pipe evacuated tubular collectors has been investigated for three different Nordic climates: Uummannaq (Greenland), Sisimiut (Greenland) and Copenhagen (Denmark). Further, the thermal performance of the evacuated tubular collectors has been compared with the thermal performance of a high efficient flat plate collector. Calculations of the yearly thermal performance show that the heat pipe evacuated tubular collectors are relatively better performing in Uummannaq than in Copenhagen compared to the flat plate collector. Further calculations assuming that no solar radiation is absorbed on the back side of the absorbers in the evacuated tubular collectors have been carried out and the performance improvement by having double-sided absorbers has been studied. Here the results for both the flat strip evacuated tubular collector and the curved strip evacuated tubular collector show that the influence of the double-sided absorber increases with increasing latitudes.

1. INTRODUCTION

This work presents theoretical investigations of how heat pipe evacuated tubular collectors can utilize the solar radiation at high latitudes. Two designs of heat pipe evacuated tubular collectors are investigated theoretically. The absorber fins in the evacuated tubes are either flat or curved and the fins have selective coating on both sides. This means that solar radiation from all directions can be utilized. The tubes are connected to a heat exchanger manifold pipe where condensers for all tubes are placed. An illustration of the evacuated tubes is given in Fig. 1.

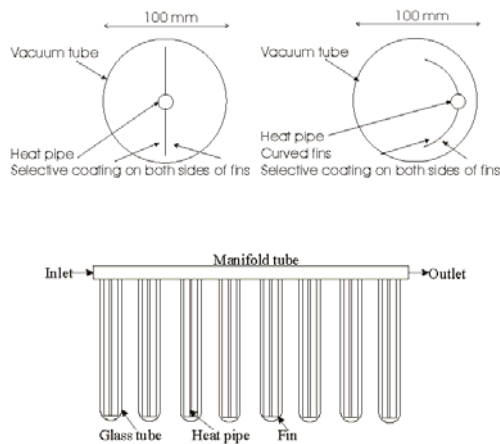


Fig. 1: The investigated evacuated tubular heat pipes.

Two new TrnSys (Klein, S.A. et al. (1996)) models for collectors with evacuated tubes with flat and curved fins have been developed. The models take solar radiation from all directions into account. Due to the cylindrical tubes, depending on the position of the sun and the distance between the tubes, the tubes will be able to cast shadow on each other as illustrated in Fig. 2. Thus, the solar irradiance can vary along the fin. Of course, for the curved fin, the irradiance always varies along the fin as the incidence angle varies along the fin. Due to this variation in the solar irradiances along the fins, the traditional fin efficiency cannot be applied and the heat transfer processes in the fin must be solved in detail.

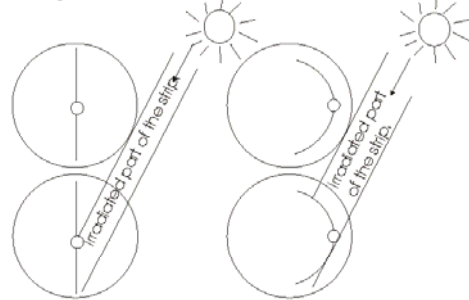


Fig. 2: The irradiated part of the fin for a given position of the sun.

The input to the model is the exact collector geometry (and not a standard efficiency expression) and it is therefore possible to determine the actual collector geometry's influence on the yearly thermal performance.

The yearly thermal performance of heat pipe evacuated tubular collectors placed in a collector field on the ground will be investigated. Therefore, shadows on the ground caused by the collector rows, and view factors including reduction of the view factors to ground and sky due to the collector rows must also be calculated in detail. This theory is included in a third TrnSys model, which works together with the two collector models.

The yearly thermal performance of heat pipe evacuated tubular collectors will be investigated for three different Nordic climates: Uummannaq (GL), Sisimiut (GL) and Copenhagen (DK). Especially, for the most Nordic locations, Uummannaq and Sisimiut, during summertime solar radiation will be present almost 24 hours a day. This means that the evacuated tubular collectors with selective coating on both sides of the absorbers might have an extra advantage compared to traditional collectors as they can utilize solar radiation from all directions.

For different collector operation conditions and different evacuated tubular collector geometries, the investigation will elucidate the influence of the double-sided absorbers on the thermal performance. Further, the performance of the evacuated tubular collectors will be compared with the performance of a high efficiency flat plate collector.

2. BACKGROUND THEORY

2.1 Heat pipe evacuated tubular collector models

The theory behind the heat pipe evacuated tubular collector models will not be described here, as it has previously been described in Shah, L.J. & Furbo, S. (2005a) and Shah, L.J. & Furbo, S. (2005b).

2.2 Collector row model

The purpose of the collector row model is to get information of the influence of the distance between collector rows on the thermal performance. The model calculates in detail:

- Shadows on the ground caused by the collector rows
- Shadows on the collectors caused by the collector rows
- Reduction of view factors from collector to ground and sky due to the collector rows
- Reduction of view factors from ground to sky due to the collector rows

In the following, the theory in the model will be described.

Shadows on the ground:

The shadows on the ground depend on the length, L , azimuth, γ_s and tilt, β , of the collector, and the solar zenith, θ_z , and solar azimuth, γ_s (see Fig. 3). The aim is to find the position of the solar part on the ground (= ground area irradiated with direct solar radiation) and thus to find

the view factor to the solar part on the ground from the collector front side ($F_{\text{col,dir,ground,front}}$) and back side ($F_{\text{col,dir,ground,back}}$). These view factors are important in order to correctly calculate the ground reflected direct solar radiation.

In vector notation, the position of the sun can be described by:

$$\vec{S} = \begin{pmatrix} \sin \theta_z \cdot \cos(\gamma_s - \gamma_f) \\ \sin \theta_z \cdot \sin(\gamma_s - \gamma_f) \\ \cos \theta_z \end{pmatrix} \quad (1)$$

The point P_0 and P_j (see Fig. 4 and Fig. 5) are given by:

$$P_0 = \begin{pmatrix} \cos(\beta) \\ \sin(\gamma_f - \gamma_r) \\ \sin(\beta) \end{pmatrix} = \begin{pmatrix} \cos(\beta) \\ 0 \\ \sin(\beta) \end{pmatrix} \quad (2)$$

$$P_j = \begin{pmatrix} x_j \\ y_j \\ z_j \end{pmatrix} = \begin{pmatrix} x_0 \\ y_0 \\ z_0 \end{pmatrix} + \begin{pmatrix} \sin \theta_z \cdot \cos(\gamma_s - \gamma_f) \\ \sin \theta_z \cdot \sin(\gamma_s - \gamma_f) \\ \cos \theta_z \end{pmatrix} \cdot X \quad (3)$$

Knowing that z_j is equal to 0 gives a solution for X and thus for x_j :

$$x_j = x_0 - \tan(\theta_z) \cdot \cos(\gamma_s - \gamma_f) \cdot z_0 \quad (4)$$

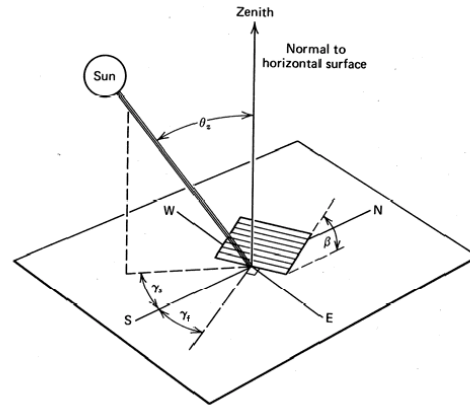


Fig. 3: Illustration of angles used in the theory (from Duffie J.A. and Beckman W.A. (1980))

If $|\gamma_s - \gamma_f|$ is less than or equal to $\pi/2$, that is if the sun shines on the front side of the collector, the view factor to the solar part on the ground from the collector front and back side is found by using the one-dimensional "string-method" (Havig S. (1986)):

$$F_{col,dir,ground,front} = \frac{dist + z - x_j - z_1}{2 \cdot L} \quad (5)$$

$$F_{col,dir,ground,back} = \frac{L + x_{sol} - z_2}{2 \cdot L} \quad (6)$$

Here “dist” is the distance between the collector rows, and z , z_1 , z_2 are given by (see Fig. 4):

$$z = \sqrt{x_j^2 + L^2 - 2 \cdot x_j \cdot L \cdot \cos(\beta)} \quad (7)$$

$$z_1 = \sqrt{dist^2 + L^2 - 2 \cdot dist \cdot L \cdot \cos(\beta)} \quad (8)$$

$$z_2 = \sqrt{x_{sol}^2 + L^2 - 2 \cdot x_{sol} \cdot L \cdot \cos(\pi - \beta)} \quad (9)$$

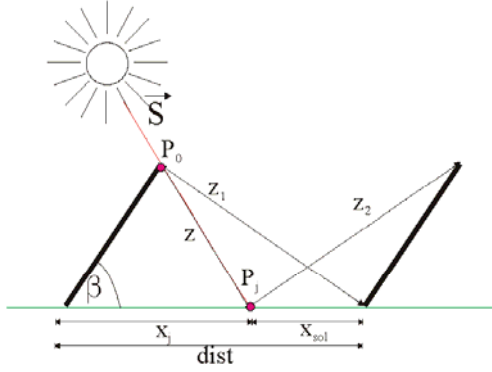


Fig. 4: The geometry used in the derivation of the view factor to the solar part on the ground from the collector when $|\gamma_s - \gamma_f|$ is less than or equal to $\pi/2$.

If $|\gamma_s - \gamma_f|$ is greater than $\pi/2$, that is if the sun shines on the back side of the collector, the view factor to the solar part on the ground from the collector front and back side is found in the following way (see Fig. 5):

$$F_{col,dir,ground,front} = \frac{dist + z_4 - x_j - z_5}{2 \cdot L} \quad (10)$$

$$F_{col,dir,ground,back} = \frac{L + x_{sol} - z_3}{2 \cdot L} \quad (11)$$

Here z_3 , z_4 and z_5 are given by:

$$z_3 = \sqrt{x_{sol}^2 + L^2 - 2 \cdot x_{sol} \cdot L \cdot \cos(\beta)} \quad (12)$$

$$z_4 = \sqrt{x_j^2 + L^2 - 2 \cdot x_j \cdot L \cdot \cos(\pi - \beta)} \quad (13)$$

$$z_5 = \sqrt{dist^2 + L^2 - 2 \cdot dist \cdot L \cdot \cos(\pi - \beta)} \quad (14)$$

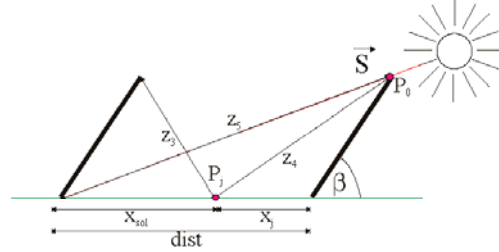


Fig. 5: The geometry used in the derivation of the view factor to the solar part on the ground from the collector when $|\gamma_s - \gamma_f|$ is greater than $\pi/2$.

Shadows due to rows on the collectors:

Furthermore, shadows on the collectors due to neighbour rows must be treated. These shadows occur when “ x_j ” is greater than “dist”. Determination of these shadows is important in order to correctly calculate the direct solar radiation on the collectors.

If $|\gamma_s - \gamma_f|$ is less than or equal to $\pi/2$, that is if the sun shines on the front side of the collector, the length of the shaded part of the collector, L_{shad} , can be described as (see Fig. 6):

$$L_{shad} = v \cdot \frac{\sin\left(\frac{\pi}{2} - \theta_z\right)}{\sin\left(\frac{\pi}{2} + \theta_z - \beta\right)} \quad (15)$$

If $|\gamma_s - \gamma_f|$ is greater than $\pi/2$, that is if the sun shines on the back side of the collector, the length of the shaded part of the collector, L_{shad} , can be described as (see Fig. 7):

$$L_{shad} = v \cdot \frac{\sin\left(\frac{\pi}{2} - \theta_z\right)}{\sin\left(\beta + \theta_z - \frac{\pi}{2}\right)} \quad (16)$$

Finally, the shade reduction factor due to shades on the collectors, can be described as:

$$F_{red_shade} = 1 - \frac{L_{shad}}{L} \quad (17)$$

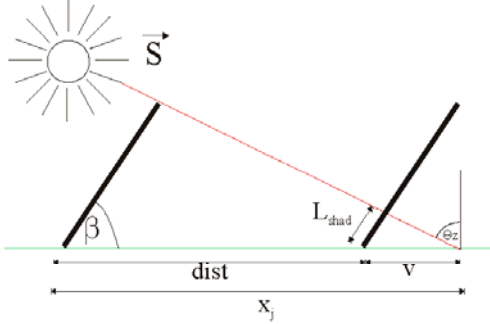


Fig. 6: The geometry used in the derivation of the shadows on the collectors when $|\gamma_s - \gamma_d|$ is less than or equal to $\pi/2$.

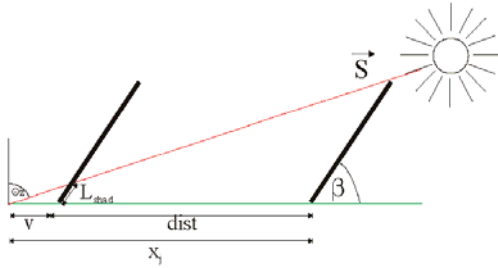


Fig. 7: The geometry used in the derivation of the shadows on the collectors when $|\gamma_s - \gamma_d|$ is greater than $\pi/2$.

Reduction due to rows of view factors for diffuse radiation:

The view factors to the ground and to the sky from the collector will be reduced due to the collector rows, compared to if there were no neighbour rows. Therefore, reduction factors for the view factors are important in order to correctly calculate the ground reflected direct solar radiation. These reduction factors can generally be described as:

$$F_{\text{reduction}} = \frac{F_{\text{collector-surrounding with rows}}}{F_{\text{collector-surrounding without rows}}} \quad (18)$$

The actual reduction factors can be described as (see Fig. 4 and Fig. 5):

$$F_{\text{red}_c_g_{\text{back}}} = \frac{0.5 \cdot (L + \text{dist} - z_1)}{\frac{L}{1 + \cos(\beta)}} = \frac{L + \text{dist} - z_1}{L \cdot (1 + \cos(\beta))} \quad (19)$$

$$F_{\text{red}_c_s_{\text{front}}} = \frac{0.5 \cdot (L + \text{dist} - z_1)}{\frac{L}{1 + \cos(\beta)}} = \frac{L + \text{dist} - z_1}{L \cdot (1 + \cos(\beta))} \quad (20)$$

$$F_{\text{red}_c_g_{\text{front}}} = \frac{0.5 \cdot (L + \text{dist} - z_5)}{\frac{L}{1 + \cos(\pi - \beta)}} = \frac{L + \text{dist} - z_5}{L \cdot (1 + \cos(\pi - \beta))} \quad (21)$$

$$F_{\text{red}_c_s_{\text{back}}} = \frac{0.5 \cdot (L + \text{dist} - z_5)}{\frac{L}{1 + \cos(\pi - \beta)}} = \frac{L + \text{dist} - z_5}{L \cdot (1 + \cos(\pi - \beta))} \quad (22)$$

Reduction due to rows of view factor from ground to sky:

Finally, the view factor from ground to sky will also be reduced due to the collector rows, and this will influence the diffuse radiation on horizontal. The view factor from ground to sky is found by:

$$F_{g-s} = \frac{z_1 + x_5 - 2 \cdot L}{2 \cdot \text{dist}} \quad (23)$$

2.3 TrnSys model

The theory described above is programmed into a TrnSys type, which works together with the heat pipe evacuated tubular collector models. The actual values used by the collector models are given in equations (5) – (6), (17) and (19) – (23).

3. CALCULATIONS

In the following calculation examples it is assumed that the ground mounted heat pipe evacuated tubular collector panels are operating in a solar heating plant at a constant operating temperature in the heat exchanger manifold pipe throughout the year.

3.1 Weather data

The yearly thermal performance of heat pipe evacuated tubular collectors will be investigated for three different Nordic climates: Uummannaq (Greenland), Sisimiut (Greenland) and Copenhagen (Denmark) as summarized in Table 1. For Uummannaq and Sisimiut, the albedo is set higher during a large part of the year due to snow on the ground.

Location	Unit	UMA (Kragh J. et al. (2005))	SIS (Unpublished)	CPH (Lund H. (1995))
Latitude	[°]	71	67	56
Longitude	[°]	52	54	-12
T_a	[°C]	-4.2	-3.7	7.8
G_{global}	[kWh/m ²]	888	827	1002
$G_{diffuse}$	[kWh/m ²]	409	352	510
Albedo	[-]	0.2 (15/6-14/9) 0.7 (15/9-14/6)	0.2 (1/5-30/9) 0.7 (1/10-30/4)	0.2 (1/1-31/12)

Table 1: Summarized data for Uummannaq (UMA), Sisimiut (SIS) and Copenhagen (CPH).

Fig. 8, Fig. 9 and Fig. 10 shows monthly values of global radiation, diffuse radiation and average ambient temperature for Uummannaq, Sisimiut and Copenhagen. As expected, the global radiation (Fig. 8) is highest in Copenhagen during the winter months. However, during April to July, the global radiation is highest in Uummannaq, which is due to a limited number of cloudy days.

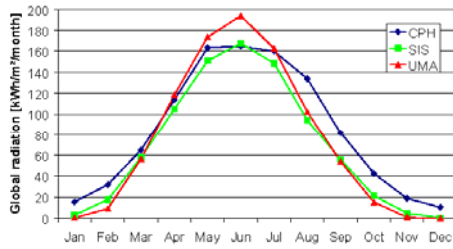


Fig. 8: Monthly values of global radiation for Uummannaq, Sisimiut and Copenhagen.

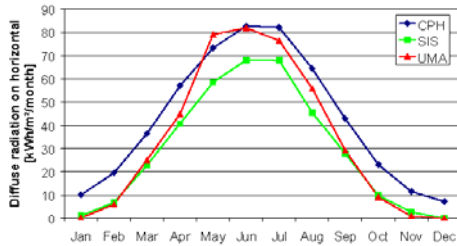


Fig. 9: Monthly values of diffuse radiation on horizontal for Uummannaq, Sisimiut and Copenhagen.

In Fig. 9 it can be seen that the diffuse radiation on horizontal is largest in Copenhagen during the whole year except for May. Comparing this to Fig. 8 shows that

especially the direct radiation on horizontal is higher in Uummannaq during April to July.

From Fig. 10 it can be seen that the monthly average ambient temperatures typically are 10 K – 15 K lower in Uummannaq and Sisimiut compared to Copenhagen.

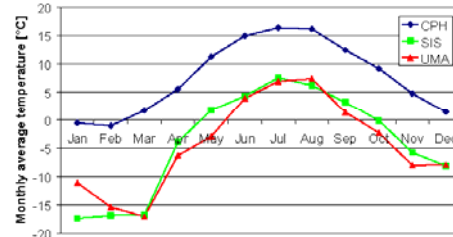


Fig. 10: Monthly average values of ambient air temperature for Uummannaq, Sisimiut and Copenhagen.

3.2 Collector input

As mentioned earlier it is assumed that the ground mounted evacuated tubular collector panels are operating in a solar heating plant at a constant operating temperature in the heat exchanger manifold pipe throughout the year. The model data of the collector panels are given in Table 2.

The performance of the heat pipe evacuated tubular collectors is compared with the performance of a high efficiency flat plate collector. The characteristic of this collector is given in Table 3.

Tube length, L	[m]	2
Glass tube outer radius	[m]	0.05
Absorber radius for curved fin	[m]	0.04375
Fin width for curved fin (corresponding to a curved fin angle of 164°)	[m]	0.125
Fin width (for flat fin)	[m]	0.0875
Fin width (for flat fin)	[m]	0.0875
Flat fin absorber area	[m ²]	0.175
Fin thickness	[m]	0.0002
Fin conductivity	[W/mK]	216
Tube centre distance	[m]	0.125
Tube heat loss coefficient based on absorber front side area	[W/m ² K]	2.43
Effective transmittance absorptance product	[-]	0.84
Incident angle modifier constant	[-]	3.8
Manifold heat loss coefficient	[W/K/m]	0.134
Manifold heat exchange rate per connection	[W/K]	10
Operating temperature in manifold	[°C]	50
Collector heat capacity	[kJ/K/tube]	1.9
Distance between collector rows	[m]	10

Table 2: Data describing the heat pipe collector in the model.

η [-]	a_0 [W/m ² K]	a_1 [W/m ² /K ²]	K_0 [-]
0.82	2.44	0.005	$1 - \tan(\theta/2)^{3.8}$

Table 3: Characteristics for the flat plate collector.

3.3 Results

The first calculations are made in order to find the optimal collector tilt for the three locations. For the flat strip heat pipe evacuated tubular collector, Fig. 11 shows the thermal performance per m² transparent area as a function of the collector tilt. For the evacuated tubular collectors, the transparent area is defined as the cross sectional area of the glass tubes. The calculations are carried out with a collector row distance of 10 m and for an average temperature of 50°C in the heat exchanger manifold pipe. It can be seen that the optimal tilt is about:

- 45° in Copenhagen
- 50° in Sisimiut
- 60° in Uummannaq

The same optimal tilts are found also to be valid for the curved strip heat pipe evacuated tubular collector and for the flat plate collector.

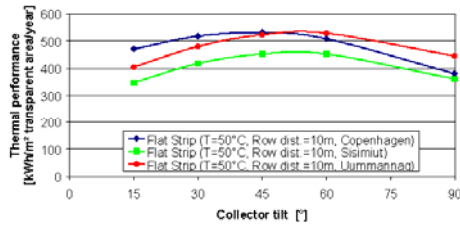


Fig. 11: Thermal performance for the heat pipe evacuated tubular collector with the flat strip as a function of the collector tilt.

To show the influence of the collector row distance, Fig. 12 shows the thermal performance for the heat pipe evacuated tubular collector with the flat strip as a function of the collector row distance. It can be seen that thermal performance increases rapidly when the row distance increases from 1 m to 10 m. Further increase in the row distance has less impact on the thermal performance. It must be noticed that the heat loss in the pipes connecting the collector rows is not included in this analysis. The reason for the increase in thermal performance is that with increasing distances:

- the view factors to solar part on the ground increases (see eq. (5)-(6), (11)-(12))
- the shadows from neighbour rows on the collector decreases (see eq. (15))
- the reduction factors for view factor from the collector to ground and sky increases (see eq. (19)-(22))
- the view factor from the ground to the sky increases (see eq. (23)).

The tendencies shown in Fig. 12 are the same for the analysis with the curved strip heat pipe evacuated tubular collector and for the flat plate collector.

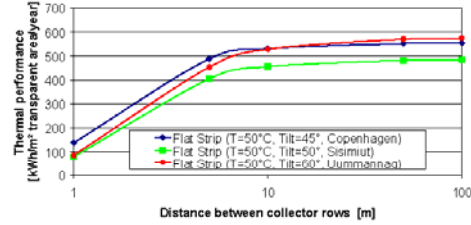


Fig. 12: Thermal performance for the heat pipe evacuated tubular collector with the flat strip as a function of the collector row distance.

For Copenhagen, Sisimiut and Uummannaq, Fig. 13, Fig. 14 and Fig. 15 show the thermal performance as a function of the operating temperature. For the flat plate collector, the operating temperature is the collector fluid mean temperature. For the heat pipe evacuated tubular collectors, the operating temperature is the collector fluid mean temperature in the heat exchanger manifold pipe.

First of all, the figures show that the thermal performance decreases with increasing temperature level, obviously due to the increasing heat loss.

Comparing the heat pipe evacuated tubular collectors with the flat and curved strips respectively; it appears that the flat strip evacuated tubular collector performs better than the curved strip evacuated tubular collector for higher temperatures. The reason is that the heat loss is larger for the curved strip collector compared to the flat strip collector as the heat loss coefficient (the same for the two collectors) is based on the absorber front side area and the curved absorber is larger than the flat fin absorber.

Comparisons of the “collector ranking” for the three locations show that in:

- Copenhagen (Fig. 13) the flat plate collector performs best for operating temperatures up to 80°C. The flat strip evacuated tubular collector performs second best for temperatures up to 80°C and the curved strip evacuated tubular collector performs third best.
- Sisimiut (Fig. 14) the flat plate collector performs best for operating temperatures up to 60°C and the flat strip evacuated tubular collector is best performing for operating temperatures over 60°C. The difference in thermal performance between the flat plate collector and the curved strip evacuated tubular collector is smaller under Sisimiut weather data compared to Copenhagen weather data.
- Uummannaq (Fig. 15) the flat strip evacuated tubular collector is best performing for almost all operating temperatures and the performances of the

flat plate collector and the curved strip evacuated tubular collector are more or less identical.

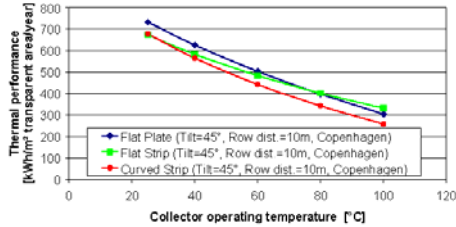


Fig. 13: The thermal performance per m² transparent area in Copenhagen as a function of the operating temperature.

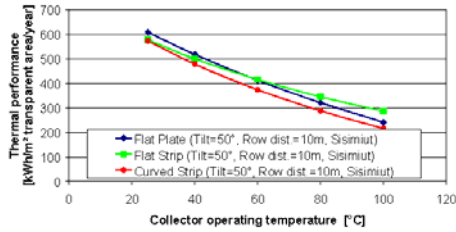


Fig. 14: The thermal performance per m² transparent area in Sisimiut as a function of the operating temperature.

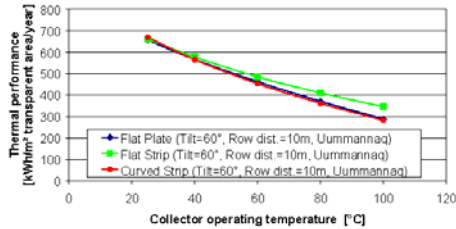


Fig. 15: The thermal performance per m² transparent area in Uummannaq as a function of the operating temperature.

In Fig. 16, Fig. 17 and Fig. 18 the thermal performances are compared in a different way. The performance of each collector type is shown as a function of the operating temperature and the location. Now it can be seen that:

- The flat strip (Fig. 16) and the curved strip (Fig. 17) evacuated tubular collectors have more or less the same thermal performances in Copenhagen and in Uummannaq.

- The flat plate collector (Fig. 18) has a lower thermal performance in Uummannaq than in Copenhagen.
- All three collectors have the lowest thermal performance in Sisimiut, which is due to the less solar radiation in Sisimiut compared to the two other locations.

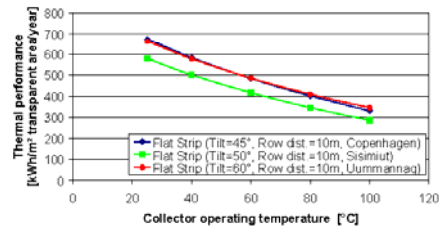


Fig. 16: Thermal performance per m² transparent area for the flat strip evacuated tubular collector as a function of the operating temperature.

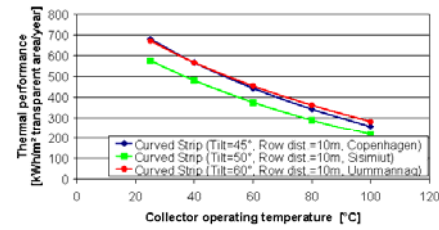


Fig. 17: Thermal performance per m² transparent area for the curved strip evacuated tubular collector as a function of the operating temperature.

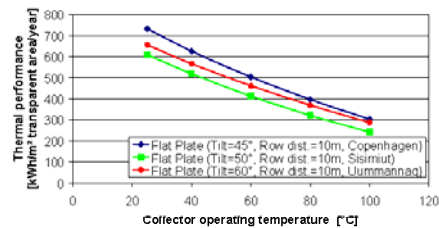


Fig. 18: Thermal performance per m² transparent area for the flat plate collector as a function of the operating temperature.

The results show that the heat pipe evacuated tubular collectors are relatively better performing in Uummannaq than in Copenhagen compared to the flat plate collector. Does this mean that the evacuated tubular collectors with

selective coating on both sides of the absorbers do have an extra advantage compared to traditional collectors due to the possibility of utilization of solar radiation from all directions? This will be investigated in the following sections.

Utilization of solar radiation in Uummannaq:

As an example Fig. 19 show the power from the three collectors in Uummannaq during the 1st of July. The weather conditions on this day are shown in Fig. 20. Here it can be seen that the solar zenith is below 90° during all 24 hours and the global radiation never goes to zero. The ambient temperature is in the range of 7°C to 13°C.

In Fig. 19 it can be seen that the period of operation for the evacuated tubular collectors is longer than the period of operation for the flat plate collector. The flat plate collector is in operation during 13 hours of the day, whereas the curved strip and the flat strip evacuated tubular collectors are in operation during respectively 18 hours and 19 hours of the day. This shows that the double sided absorbers do have an influence.

The figure also shows that the thermal performance of the flat plate collector is superior to the evacuated tubular collectors during mid-day. Further, it can be seen that the curved strip evacuated tubular collector, which has the lowest performance during mid-day, has the highest performance in the morning and in the afternoon. The reason for this is mainly related to the incidence angle.

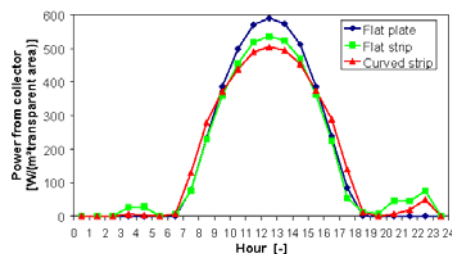


Fig. 19: The power from the three collectors in Uummannaq during the 1st of July.

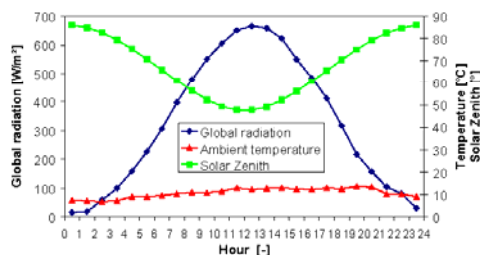


Fig. 20: Weather conditions on the 1st of July in Uummannaq.

For the investigated day, the accumulated thermal performances are 4.1 kWh/m² transparent area for the curved strip evacuated tubular collector; 4.1 kWh/m² transparent area for the flat strip evacuated tubular collector and 4.2 kWh/m² transparent area for the flat plate evacuated tubular collector.

Influence of the double-sided absorbers:

To further investigate the influence of the double-sided absorbers, calculations assuming that no solar radiation is absorbed on the back side of the absorbers in the evacuated tubular collectors have been carried out.

Fig. 21, Fig. 22 and Fig. 23 show the thermal performance as a function of the operating temperature for the three locations. The figures can be compared to Fig. 13, Fig. 14 and Fig. 15. The only difference in the calculations is that the evacuated tubular collectors with both flat and curved strips do not absorb solar radiation on the strip back side.

Comparisons the “collector ranking” for the three locations now show that the flat plate collector is best performing, the flat strip evacuated tubular collector is second best performing and the curved strip evacuated tubular collector has the lowest thermal performance. Thus, it is clearly illustrated that the solar radiation on the back side of the absorbers has a significant influence on the thermal performance.

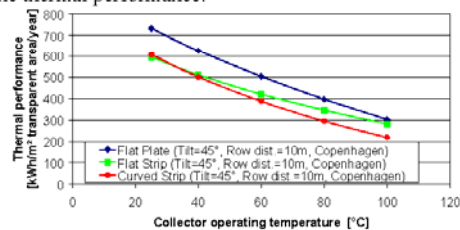


Fig. 21: The thermal performance per m² transparent area in Copenhagen as a function of the operating temperature. Here the evacuated tubular collectors with both flat and curved strips do NOT absorb solar radiation on the strip back side.

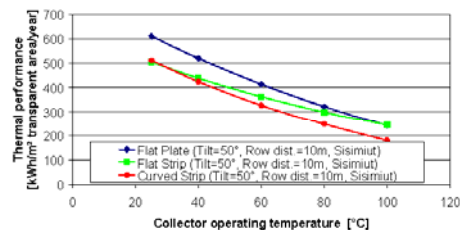


Fig. 22: The thermal performance per m² transparent area in Sisimiut as a function of the operating temperature. Here the evacuated tubular collectors with both flat and curved strips do NOT absorb solar radiation on the strip back side.

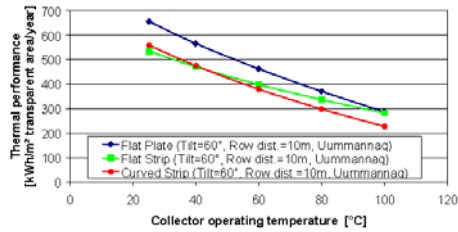


Fig. 23: The thermal performance per m² transparent area in Uummannaq as a function of the operating temperature. Here the evacuated tubular collectors with both flat and curved strips do NOT absorb solar radiation on the strip back side.

The quantitative influence of the double-sided absorbers is shown in Fig. 24 and Fig. 25 where the relative thermal performances for respectively the flat and the curved strip evacuated tubular collector are shown as a function of the operating temperature.

Here the relative thermal performance, ψ , is defined as the thermal performance of the double-sided evacuated tubular collector divided by the thermal performance of the single-sided evacuated tubular collector:

$$\psi = \frac{\text{Performance}_{\text{double-sided absorber}}}{\text{Performance}_{\text{single-sided absorber}}} \quad (24)$$

For both the flat strip evacuated tubular collector (Fig. 24) and the curved strip evacuated tubular collector (Fig. 25), it can be seen that the influence of the double-sided absorber increases with increasing latitudes. For example, in Uummannaq for a collector operating temperature of 60°C the extra thermal performance is about 22% for the flat strip evacuated tubular collector and about 19% for the curved strip evacuated tubular collector. In Copenhagen, at the same temperature level, the extra thermal performances are about 15% for the flat strip evacuated tubular collector and about 14% for the curved strip evacuated tubular collector.

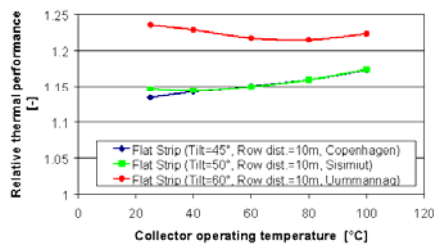


Fig. 24: The relative thermal performance for the flat strip evacuated tubular collector as a function of the operating temperature.

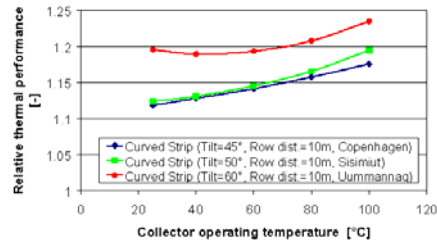


Fig. 25: The relative thermal performance for the curved strip evacuated tubular collector as a function of the operating temperature.

4. CONCLUSIONS

Theoretical investigations of how two differently designed ground mounted heat pipe evacuated tubular collectors utilize the solar radiation at high latitudes have been carried out. The absorber fins in the evacuated tubes are either flat or curved and the fins have selective coating on both sides so that solar radiation from all directions can be utilized.

The yearly thermal performance of heat pipe evacuated tubular collectors has been investigated for three different Nordic climates: Uummannaq (Greenland), Sisimiut (Greenland) and Copenhagen (Denmark). Further, the performance of the evacuated tubular collectors has been compared with the performance of a high efficient flat plate collector.

Calculations of the yearly thermal performance show that the heat pipe evacuated tubular collectors are relatively better performing in Uummannaq than in Copenhagen compared to the flat plate collector.

Further, a detail analysis of the collector operation on a summer day in Uummannaq show that the period of operation for the evacuated tubular collectors is longer than the period of operation for the flat plate collector. Assuming a operating temperature of 50°C, the flat plate collector is in operation during 13 hours of the day, whereas the curved strip and the flat strip evacuated tubular collectors are in operation during 18 hours and 19 hours of the day, respectively.

To further investigate the influence of the double-sided absorbers, calculations assuming that no solar radiation is absorbed on the back side of the absorbers in the evacuated tubular collectors have been carried out and the performance improvement by having double-sided absorbers has been studied.

Here the results for both the flat strip evacuated tubular collector and the curved strip evacuated tubular collector show that the influence of the double-sided absorber increases with increasing latitudes. Thus, in Uummannaq for a collector operating temperature of 60°C the extra thermal performance is about 22% for the flat strip evacuated tubular collector and about 19% for the curved strip evacuated tubular collector. In Copenhagen at the

same temperature the extra thermal performances are about 15% for the flat strip evacuated tubular collector and about 14% for the curved strip evacuated tubular collector.

Further work:

Parallel to the theoretical work, the investigated heat pipe evacuated tubular collectors will be tested side-by-side in an outdoor test facility. The measured performances will be used to verify the theoretical models.

ACKNOWLEDGEMENTS

This study is financed by the VILLUM KANN RASMUSSEN FOUNDATION.

NOMENCLATURE

dist	Distance between collector rows, m
$F_{col,dir,ground,back}$	View factor from the collector back side to the part of the ground with direct solar radiation, -
$F_{col,dir,ground,front}$	View factor from the collector front side to the part of the ground with direct solar radiation, -
$F_{ground,sky}$	View factor from the ground to the sky, -
$F_{red_c_g_back}$	Reduction factor from the collector back side to the part of the ground with diffuse solar radiation, -
$F_{red_c_g_front}$	Reduction factor from the collector front side to the part of the ground with diffuse solar radiation, -
$F_{red_c_s_back}$	Reduction factor from the collector back side to the sky, -
$F_{red_c_s_front}$	Reduction factor from the collector front side to the sky, -
F_{red_shade}	Shade reduction factor due to shades on the collectors, -
$F_{reduction}$	Reduction factor, -
$G_{diffuse}$	Yearly diffuse radiation on horizontal, kWh/m ²
G_{global}	Yearly global radiation, kWh/m ²
L	Tube length, m
L_{shad}	Length of shade on collector, -
P_0	Point on top of collector row, -
P_j	Point on ground, -
r_c	Glass tube radius, m
r_p	Absorber radius for curved fin, m
\vec{S}	Solar vector, -
T_a	Yearly average ambient temperature, °C
v	Help variable, m
w_c	Fin width for curved fin, m
w_f	Fin width for flat fin, m
X	Help variable, m
x_0	x coordinate of point P_0 , m
x_j	x coordinate of point P_j , m

x_{sol}	Length of solar irradiated part of ground, m
y_0	y coordinate of point P_0 , m
y_j	y coordinate of point P_j , m
z	Help variable, m
z_0	z coordinate of point P_0 , m
z_1	Help variable, m
z_2	Help variable, m
z_3	Help variable, m
z_4	Help variable, m
z_5	Help variable, m
z_j	z coordinate of point P_j , m
β	Collector row tilt, °
γ_f	Collector azimuth, °
γ_s	Solar azimuth, °
θ_z	Solar zenith, °
ψ	Relative thermal performance, -

REFERENCES

- Klein, S.A. et al. (1996). TRNSYS 14.2, User Manual. *University of Wisconsin Solar Energy Laboratory*.
- Shah, L.J. & Furbo, S. (2005a). Modelling Shadows on Evacuated Tubular Collectors with Cylindrical Absorbers. *Journal of Solar Energy Engineering, Transactions of the ASME. In press*.
- Shah, L.J. & Furbo, S. (2005b). Theoretical Investigations of differently designed Heat Pipe Evacuated Tubular Collectors. *Proceedings of ISES Solar World Congress, 6-12 August, Orlando, Florida, USA. In press*.
- Duffie J.A. and Beckman W.A. (1980) Solar Engineering of Thermal Processes, p. 11. *Wiley Interscience, New York*.
- Hadvig S. (1986) Termisk stråling for ingeniører, pp. 89-90. *Polyteknisk Forlag, ISBN 87-502-0640-0*.
- Kragh J. et al. (2005) Weather test reference years of Greenland, *Proceedings of Nordic Symposium on Building Physics, Reykjavik 13-15 June 2005. In press*.
- Lund H. (1995). The Design Reference Year user manual. Report of IEA-SHC Task 9. Report 274. *Thermal Insulation Laboratory. Technical University of Denmark*.

Bilag 2: Solar World Congress 2005 paper: Theoretical investigations of differently designed heat pipe evacuated tubular collectors.

THEORETICAL INVESTIGATIONS OF DIFFERENTLY DESIGNED HEAT PIPE EVACUATED TUBULAR COLLECTORS

Louise Jivan Shah and Simon Furbo
Department of Civil Engineering
Technical University of Denmark
DK-2800 Kgs. Lyngby
Denmark
E-mail: ljs@byg.dtu.dk

ABSTRACT

Two designs of ground mounted heat pipe evacuated tubular collectors operating in a solar heating plant are investigated theoretically. The absorber fins inside the evacuated tubes are either flat or curved and the surfaces of the fins have selective coating on both sides. Two new TrnSys models for evacuated tubular collectors are developed. The models calculate in detail the heat transfer processes of the absorber fins.

It is illustrated how the model can be used for geometrical parameter studies. For example, it is investigated how fin geometry, collector tilt, operating temperature, tube distances and distances between collector rows influences the yearly thermal collector performance.

1 INTRODUCTION

Evacuated tubular collectors have an increasing share of the collector market in the world. Up to 2001 more than 100 million m² collectors were installed world wide. Of this, about 28% were unglazed collectors, 49% were traditional flat plate collectors and about 22% were evacuated tubular collectors. On the world largest solar thermal market, China, evacuated tubular collectors have today a market share greater than 80% [1].

Due to the market development, new collector designs as well as development of theoretical models for these designs becomes more and more important.

In this paper, two designs of heat pipe evacuated tubular collectors are investigated theoretically. The absorber fins in the evacuated tubes are either flat or curved and the fins have selective coating on both sides. This means that solar radiation from all directions can be utilized.

An illustration of the evacuated tubes is given in Fig. 1. The tubes are connected to a heat exchanger manifold pipe where condensers for all tubes are placed.

Two new TrnSys [2] models for collectors with evacuated tubes with flat and curved fins are developed. The models take solar radiation from all directions into account. Further, due to the cylindrical tubes, depending on the position of the sun and the distance between the tubes, the tubes will be able to cast shadow on each

other as illustrated in Fig. 2 and the solar irradiance can vary along the fin. For the curved fin model, the irradiance always varies along the fin as the incidence angle varies along the fin. Due to the variation in the solar irradiances along the fins, the traditional fin efficiency cannot be applied. Therefore, the heat transfer processes in the fin are solved in detail.

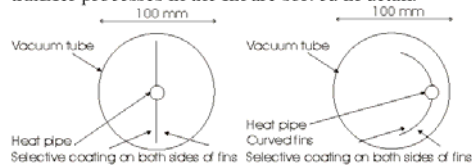


Fig. 1: The investigated evacuated tubular heat pipes.

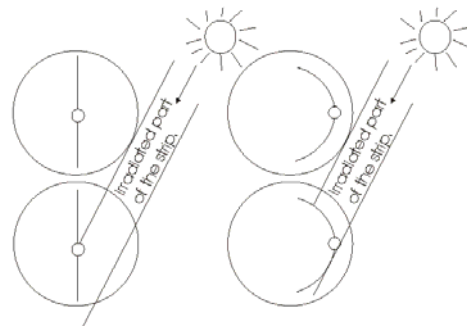


Fig. 2: The irradiated part of the fin for a given position of the sun.

With the models, a *parameter sensitivity analysis* is carried out for the evacuated tubular collectors installed in a solar heating plant. This analysis illuminates how the:

- different fin geometries
- collector tilt
- operating temperature
- tube distances
- distances between collector rows

influence the yearly thermal performance of the collector field.

2 THEORY AND DEFINITIONS

In this section, the theory of the two collector models, for flat and curved fins respectively, will be summarized. The models are developed for the TrnSys simulation program. The models include both the evacuated tubular collectors and the heat exchanger manifold pipe, as illustrated in Fig. 3.

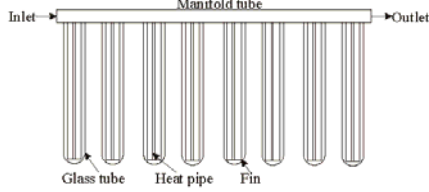


Fig. 3: The collector models include both the evacuated tubular collectors and the heat exchanger manifold pipe.

The power, P_u , from this system can be written as:

$$P_u = m \cdot c_p \cdot (T_{\text{manifold,outlet}} - T_{\text{manifold,inlet}}) \quad (1)$$

$$P_u = P_{\text{ETC}} - P_{\text{loss}} - \frac{dQ_{\text{manifold}}}{dt} \quad (2)$$

The power from the heat pipes, P_{ETC} , the heat loss from the manifold tube, P_{loss} , and the energy change in the manifold tube, dQ_{manifold} , can be written as:

$$P_{\text{ETC}} = UA_{\text{manifold}} \cdot (T_{\text{heatpipe}} - T_{\text{manifold}}) \quad (3)$$

$$P_{\text{loss}} = U_{\text{loss}} \cdot (T_{\text{manifold}} - T_{\text{amb}}) \quad (4)$$

with

$$T_{\text{manifold}} = \frac{T_{\text{manifold,inlet}} + T_{\text{manifold,outlet}}}{2} \quad (5)$$

The power from the heat pipes, P_{ETC} , is larger than zero if the temperature of the heat pipe working fluid, T_{heatpipe} , is larger than the lowest evaporation temperature and larger than the mean temperature in the manifold pipe, T_{manifold} . In other cases, P_{ETC} is zero.

In order to determine the temperature of the heat pipe working fluid, the fin is discretized into a number of elements as illustrated in Fig. 4. The energy balances for the elements of the fin are:

$$i=1: \quad -\frac{\lambda \cdot \delta}{dx} \cdot L \cdot (T_i - T_{i+1}) + S_i \cdot L \cdot dx - U_L \cdot (T_i - T_{\text{amb}}) \cdot L \cdot dx \quad (6)$$

$$= \frac{m_{\text{fin}} \cdot c_{p,\text{fin}}}{dt} \cdot (T_i^{\text{new}} - T_i^{\text{old}}) \\ 1 < i < n: \quad \frac{\lambda \cdot \delta}{dx} \cdot L \cdot (T_i - T_{i-1}) - \frac{\lambda \cdot \delta}{dx} \cdot L \cdot (T_i - T_{i+1}) + S_i \cdot L \cdot dx - U_L \cdot (T_i - T_{\text{amb}}) \cdot L \cdot dx \quad (7) \\ = \frac{m_{\text{fin}} \cdot c_{p,\text{fin}}}{dt} \cdot (T_i^{\text{new}} - T_i^{\text{old}})$$

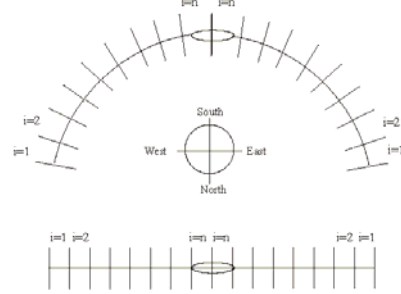


Fig. 4: The fins are discretized into a number of elements.

$$i=n: \quad \frac{\lambda \cdot \delta}{dx} \cdot L \cdot (T_i - T_{i-1}) - UA_{\text{manifold}} \cdot (T_i - T_{\text{manifold}}) + S_i \cdot L \cdot dx - U_L \cdot (T_i - T_{\text{amb}}) \cdot L \cdot dx \quad (8) \\ = \frac{m_{\text{fluid}} \cdot c_{p,\text{fluid}}}{dt} \cdot (T_i^{\text{new}} - T_i^{\text{old}})$$

Here, the solar radiation absorbed on the fin, S_i , is dependent on the position on the fin, due to varying incident angles (for curved fins) and due to possible shadows on the fin (for both flat and curved fins). The principles of determining the size and position on the fin of the shadows are described in [3].

The heat exchange capacity rate, UA_{manifold} , has a constant value larger than zero if T_n is larger than the lowest evaporation temperature and if T_n is larger than the mean temperature in the manifold pipe. In other cases, UA_{manifold} is zero.

2.1 Solar radiation and view factors

The total solar radiation absorbed on the fin, S_i , can be written as:

$$S_i = S_{i,\text{dir,front}} + S_{i,\text{dir,back}} + S_{i,\text{dif,sky,front}} + S_{i,\text{dif,sky,back}} + S_{i,\text{dir,ground,front}} + S_{i,\text{dir,ground,back}} + S_{i,\text{dif,ground,front}} + S_{i,\text{dif,ground,back}} \quad (9)$$

where,

$$S_{i,\text{dir,front}} = (\tau\alpha)_e \cdot G_b \cdot K_{\theta} \cdot R_{b,\text{front}} \cdot R_{\text{sun}} \quad (10)$$

$$S_{i,\text{dir,back}} = (\tau\alpha)_e \cdot G_b \cdot K_{\theta} \cdot R_{b,\text{back}} \cdot R_{\text{sun}} \quad (11)$$

$$S_{i,\text{dif,sky,front}} = (\tau\alpha)_e \cdot G_d \cdot K_{\theta,\text{dif}} \cdot F_{\text{col,sky,front}} \quad (12)$$

$$S_{i,\text{dif,sky,back}} = (\tau\alpha)_e \cdot G_d \cdot K_{\theta,\text{dif}} \cdot F_{\text{col,sky,back}} \quad (13)$$

$$S_{i,\text{dir,ground,front}} = (\tau\alpha)_e \cdot G_b \cdot K_{\theta,\text{gr}} \cdot F_{\text{col,dir,ground,front}} \cdot \rho$$

$$S_{i,\text{dir,ground,back}} = (\tau\alpha)_e \cdot G_b \cdot K_{\theta,\text{gr}} \cdot F_{\text{col,dir,ground,back}} \cdot \rho$$

$$S_{i,\text{dif,ground,front}} = (\tau\alpha)_e \cdot G_d \cdot F_{\text{ground,sky}} \cdot K_{\theta,\text{gr}} \cdot F_{\text{col,dif,ground,front}} \cdot \rho$$

$$S_{i,\text{dif,ground,back}} = (\tau\alpha)_e \cdot G_d \cdot F_{\text{ground,sky}} \cdot K_{\theta,\text{gr}} \cdot F_{\text{col,dif,ground,back}} \cdot \rho \quad (13)$$

The incident angle modifier K_{θ} is calculated by:

$$K_{\theta} = 1 - \tan^a\left(\frac{\theta}{2}\right) \quad (14)$$

Here, the incident angle, θ , is defined as the incident angle on the absorber. The incident angle modifiers for diffuse radiation, $K_{\theta, \text{diff}}$, and ground reflected radiation, $K_{\theta, \text{gr}}$, are evaluated by equation (14) using $\theta = \pi/3$ [4]. An illustration of the view factors is given in Fig. 5 and a more detailed description of the view factors including reduction of the view factors to ground and sky due to the collector rows, is given in [5].

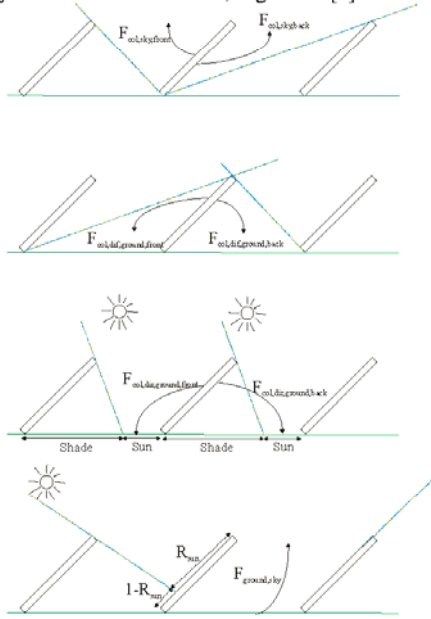


Fig. 5: An illustration, based on three collector rows, of the view factors used in the model. R_{sun} includes the effect of one row shadowing the next row.

2.2 Numerical issues

In order to evaluate the performance of the evacuated tubular collectors on an annual basis, the above theory is implemented into three TrnSys types; two TrnSys types for the two collector designs and an additional TrnSys type for the view factor calculations. Concerning the two collector types, for each simulation time step the equations (1)-(8) are solved through an iteration loop. The iteration is stopped when the fin temperature difference from iteration to iteration is less than 0.00001 K and when the difference from iteration to iteration in power from the manifold is less than 0.01 W. If the criteria are not reached the iteration loop stops after 100,000 iterations, and a warning is written to an output file. This seldom happens and the influence on the final result is insignificant. The fins are discretized into nine elements (18 elements in total), and a typical annual simulation of a collector array takes

approximately 3 min. on a 2.8 GHz PC when a timestep of 0.05 h is used.

3 PARAMETER VARIATIONS

In this section, it is illustrated how the model can be used for geometrical parameter studies. In the following examples it is assumed that the ground mounted evacuated tubular collector panels are operating in a solar heating plant at a constant operating temperature of 50°C in the heat exchanger manifold pipe throughout the year. The model data of the collector panel is given in Table 1. The collector performance is investigated for Uummanaq, Greenland, as summarized in Table 2. The albedo is set higher during a large part of the year due to snow on the ground.

TABLE 1: DATA DESCRIBING THE COLLECTOR IN THE MODEL.

Tube length, L	[m]	2
Glass tube radius, r_c	[m]	0.05
Absorber radius for curved fin, r_p	[m]	0.04375
Fin width for curved fin, w_c (corresponding to a curved fin angle of 164°)	[m]	0.125
Fin width (for flat fin), w_f	[m]	0.0875
Flat fin absorber area	[m²]	0.175
Curved fin absorber area	[m²]	0.25
Fin thickness	[m]	0.0002
Fin conductivity, k_{fin}	[W/mK]	216
Tube centre distance, C	[m]	0.125
Tube heat loss coefficient, k_{tube} based on absorber front side area	[W/m²K]	2.43
Effective transmittance absorptance product, $(\tau\alpha)_e$	[-]	0.84
Incident angle modifier constant, a	[-]	3.8
Manifold heat loss coefficient, k_{manifold}	[W/K/m]	0.134
Manifold heat exchange rate per connection, UA_{manifold}	[W/K]	10
Operating temperature in manifold	[°C]	50
Collector heat capacity, $C_{\text{collector}}$	[kJ/K/tube]	1.9
Distance between collector rows	[m]	10

TABLE 2: SUMMARIZED DATA FOR UUMMANAQ, GREENLAND.

Location	Unit	Uummanaq, GL [6]
Latitude	[°]	71
Longitude	[°]	52
T_{average}	[°C]	-4.2
G_{global}	[kWh/m²]	888
G_{direct}	[kWh/m²]	409
Albedo	[-]	0.2 (15/6-14/9) 0.7 (15/9-14/6)

3.1 View factors

To get an understanding of the geometry included in the models, illustrations of some of the view factors for different conditions is given below. The view factors are calculated for a collector tilt of 60° and for infinite distance between the collector rows.

For different tube centre distances Fig. 6 and Fig. 7 shows the view factor from one tube to the two neighbour tubes, $F_{\text{tube,tube}}$, and the view factors to the sky

and ground from the collector's front and back side respectively.

For the collector front side, it can be seen that the flat fin collector has a larger view factor to the sky, a smaller view factor to the ground and a smaller view factor between the tubes compared to the curved fin collector. This is because parts of the curved fin – due to the curve – face the neighbour tubes and the ground more than the flat fin. Further, as expected, the view factors between the tubes decreases with increasing tube centre distances. For the collector back side, it can be seen that the curves for the sky and ground radiation are parallel. The reason for this is that, when calculating the view factors, the back side of the curved fin can be treated as a flat fin placed in the opening of the curved fin. Thus the actual differences in the values are directly related to the area of the opening compared to the area of curved fin absorber. The opening area equals 69% of the curved fin absorber area.

Fig. 8 shows the yearly diffuse sky and ground reflected radiation absorbed by the fins. For the collector back side, it can be seen that, there is almost no differences between the curved and the flat fin. For the collector front side it is clear that the curved fin absorbs more diffuse radiation than the flat fin even though the view factor between fin and sky is largest for the flat fin. The reason is that the area of the curved fin is larger than the area of the flat fin.

Finally, Fig. 9 shows the direct radiation absorbed by the front side of the fins. Even though the view factor between fin and sky is largest for the flat fin, the curved fin absorbs more direct radiation per tube than the flat fin absorbs. This is still due to the larger curved fin absorber area.

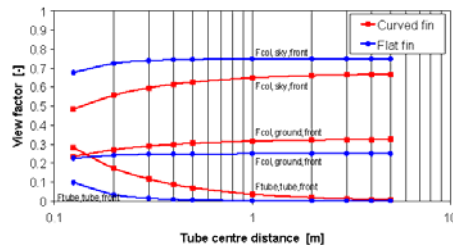


Fig. 6: View factors for the collector front side.

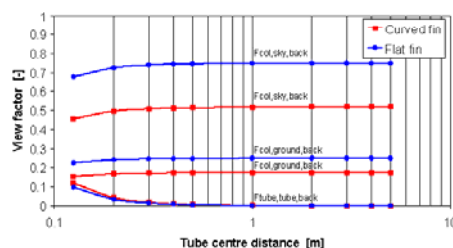


Fig. 7: View factors for the collector back side.

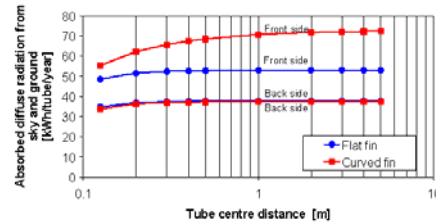


Fig. 8: Absorbed diffuse sky and ground reflected radiation.

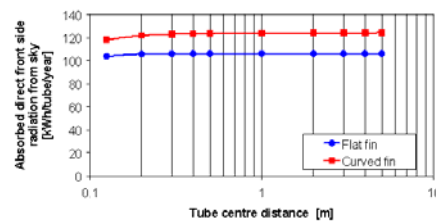


Fig. 9: Absorbed direct radiation.

3.2 Temperature profiles on the fin

Before going into thermal performance analyses, some examples of the temperature distribution on the fins are given. For a summer day (31/7), Fig. 10 and Fig. 11 show the temperature profile at solar time 9 AM, 12 PM and 3 PM for the curved and the flat fin respectively. At these three times there are no shadows from the neighbour tubes. The temperature distribution on the curved fin is symmetrical around the heat pipe at 12 PM whereas the east side of the fin is warmer during the morning and the west side of the fin is warmer during the afternoon. This clearly illustrates the influence of the distribution of the solar radiation on the fin and it explains why the traditional fin efficiency, F , cannot be applied when analysing this type of collector in detail. As expected for the flat fin, there is symmetry in the temperature distribution at all three times. The differences in the temperature level for the three times are due to the weather conditions.

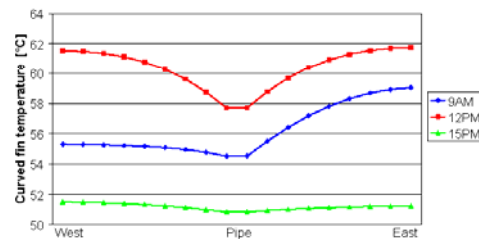


Fig. 10: The temperature distribution on the curved fin in the morning, at noon and in the afternoon of a summer day.

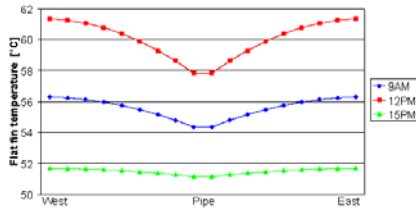


Fig. 11: The temperature distribution on the flat fin in the morning, at noon and in the afternoon.

3.3 Collector tilt

Fig. 12 shows the thermal performance per tube as a function of the collector tilt. The figure shows that the optimum tilt is about 60° for both the flat fin collector and for the curved fin collector.

The flat fin collector performs slightly better than the curved fin collector even though the curved fin absorber area is larger than the flat fin absorber area. The reason is that the heat loss is larger for the curved fin collector compared to the flat fin collector as the heat loss coefficient (the same for the two collectors) is based on the absorber front side area and the curved absorber is larger than the flat fin absorber.

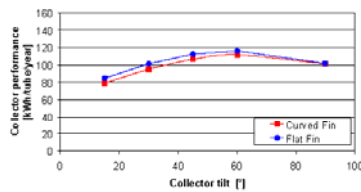


Fig. 12: The thermal performance per tube as a function of the collector tilt.

3.4 Operating temperature

Fig. 13 shows the thermal performance as a function of the operating temperature in the manifold tube. As expected the thermal performance decreases with increasing temperature level due to the increasing heat loss.

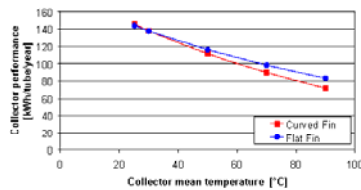


Fig. 13: The thermal performance per tube as a function of the operating temperature in the manifold tube.

Further, it can be seen that the curves cross at a temperature of approximately 30°C . Again, the reason is that the curved fin collector has a higher heat loss compared to the flat fin collector. So, for lower temperatures the extra absorber area is an advantage for

the curved fin collector and for higher temperatures the extra absorber area is a disadvantage for the curved fin collector.

3.5 Tube centre distances

Fig. 14 shows the thermal performance per tube as a function of the tube centre distance. The thermal performance increases for increasing tube centre distances up to about 0.3 m, due to reduced shaded areas, reduced view factors between the tubes and thus increased view factors to sky and ground. For even larger distances the utilized energy decreases again, due to the increasing heat loss from the manifold pipes.

Further, the curved fin collector is more sensitive to the tube centre distance compared to the flat fin collector. The reason is directly related to the differences in the view factors for the two collectors as the curved fin absorber, due to the design, “sees” more of the neighbour tubes (see $F_{\text{tube,tube}}$ in Fig. 6) for smaller tube centre distances.

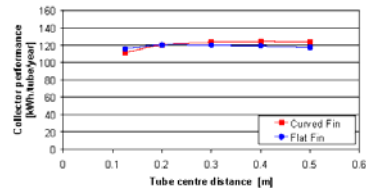


Fig. 14: The thermal performance per tube as a function of the tube centre distance.

3.6 Collector rows distances

Finally, Fig. 15 shows the thermal performance per tube as a function of the distance between the collector rows. It can be seen that thermal performance increases rapidly when the row distance increases from 1 m to 10 m. Further increase in the row distance has less impact on the thermal performance. The reason for the increase in thermal performance is that with increasing distances the shadows from neighbour rows on the collector (see Fig. 5 bottom) decreases and the view factor from the collector to ground and sky increases. It must be noticed that the heat loss in the pipes connecting the collector rows is not included in this analysis.

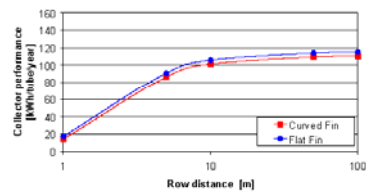


Fig. 15: The thermal performance per tube as a function of the distance between the collector rows.

4 CONCLUSION AND OUTLOOK

Two heat pipe evacuated tubular collectors operating in a solar heating plant are investigated theoretically. The

absorber fins in the evacuated tubes are either flat or curved and the fins have selective coating on both sides. Two new TrnSys models for collectors with the tubes with the flat and curved fins are developed. The models are able to take solar radiation from all directions into account. On each tube the model determines the size and position of the shadows caused by the neighbour tube as a function of the solar azimuth and zenith, and the temperature profiles on the fins are calculated in detail. Further, based on the tube geometry, the collector tilt and the distances between collector rows in the collector array of a solar heating plant, view factors between the tubes and from the collector to ground and sky are calculated in detail.

It is illustrated how the model can be used for geometrical parameter studies, where the evacuated tubular collectors are operating in a solar heating plant. For example, it is investigated how the fin geometry, collector tilt, operating temperature, tube distances and distances between collector rows influences the yearly thermal collector performance.

Further work:

Parallel to the theoretical work, the investigated heat pipe evacuated tubular collectors will be tested side-by-side in an outdoor test facility. The measured performances will be used to verify the TrnSys models.

5 NOMENCLATURE

a	Incident angle modifier constant, -
C	Tube centre distance, m
$C_{collector}$	Collector heat capacity, kJ/K/tube
$C_{p,fin}$	Heat capacity of fin material, J/kgK
$C_{p,fluid*}$	Average heat capacity of fin material and working fluid in heat pipe, J/kgK
$dQ_{manifold}$	Energy change in the manifold pipe, J
dt	Time step, s
dx	Width of discretization element, m
$F_{col,dif,ground,back}$	View factor from the collector back side to the part of the ground with diffuse solar radiation, -
$F_{col,dif,ground,front}$	View factor from the collector front side to the part of the ground with diffuse solar radiation, -
$F_{col,dir,ground,back}$	View factor from the collector back side to the part of the ground with direct solar radiation, -
$F_{col,dir,ground,front}$	View factor from the collector front side to the part of the ground with direct solar radiation, -
$F_{col,sky,back}$	View factor from the collector back side to the sky, -
$F_{col,sky,front}$	View factor from the collector front side to the sky, -
$F_{ground,sky}$	View factor from the ground to the sky, -
$F_{tube,tube}$	View factor from one tube to the neighbour tubes, -
G_b	Beam radiation on horizontal, W/m ²
G_d	Diffuse radiation on horizontal, W/m ²
$G_{diffuse}$	Yearly diffuse radiation on horizontal, kWh/m ²
G_{global}	Yearly global radiation, kWh/m ²
K_θ	Incident angle modifier for direct radiation, -
$K_{\theta,dif}$	Incident angle modifier for diffuse radiation, -
$K_{\theta,gr}$	Incident angle modifier for gr. reflected radiation, -
L	Tube length, m
m_{fin}	Mass of discretized fin element, kg
m_{fluid*}	Average mass of fin material and working fluid in heat pipe, kg
P_{ETC}	Power from heat pipes, W
P_{loss}	Heat loss from the manifold pipe, W
P_u	Power from collector, W
$R_{b,back}$	Geometric factor for back side beam radiation, -
$R_{b,front}$	Geometric factor for front side beam radiation, -
r_c	Glass tube radius, m
r_p	Absorber radius for curved fin, m

R_{sun}	Part of tube irradiated by direct radiation due to row shadows, -
S_i	solar radiation absorbed on element i, W/m ²
$S_{i,dif,sky,front}$	Diffuse sky radiation absorbed on the absorber front side, W/m ²
$S_{i,dif,ground,back}$	Ground reflected diffuse radiation absorbed on the absorber back side, W/m ²
$S_{i,dif,ground,front}$	Ground reflected diffuse radiation absorbed on the absorber front side, W/m ²
$S_{i,dif,sky,back}$	Diffuse sky radiation absorbed on the absorber back side, W/m ²
$S_{i,dir,back}$	Direct radiation absorbed on the absorber back side, W/m ²
$S_{i,dir,front}$	Direct radiation absorbed on the absorber front side, W/m ²
$S_{i,dir,ground,front}$	Ground reflected direct radiation absorbed on the absorber front side, W/m ²
$S_{i,dir,ground,back}$	Ground reflected direct radiation absorbed on the absorber front side, W/m ²
$T_{a,average}$	Yearly average ambient temperature, °C
T_{amb}	Ambient temperature, °C
T_{amb}	Ambient temperature, °C
$T_{heatpipe}$	Temperature of the heat pipe working fluid, °C
T_i	Temperature of element i, °C
T_{i+1}	Temperature of element i+1, °C
T_{i-1}	Temperature of element i-1, °C
T_i^{new}	New temperature of element i, °C
T_i^{old}	Old temperature of element i, °C
$T_{manifold}$	Mean temperature in manifold, °C
$T_{manifold,inlet}$	Inlet temperature to manifold, °C
$T_{manifold,outlet}$	Outlet temperature from manifold, °C
$UA_{manifold}$	Manifold heat exchange rate, W/K
U_L	Tube heat loss coefficient, W/m ² K
U_{loss}	Manifold heat loss coefficient, W/K/m
w_c	Fin width for curved fin, m
w_f	Fin width for flat fin, m
δ	Fin thickness, m
λ	Fin thermal conductivity, W/mK
ρ	Ground albedo, -
$(\tau\alpha)_e$	Effective transmittance absorptance product, -

6 ACKNOWLEDGEMENTS

This study is financed by the VILLUM KANN RASMUSSEN FOUNDATION.

7 REFERENCES

- (1) Weiss W., Bergmann I., Faninger G., "Solar Heating Worldwide. Markets and Contributions to the Energy Supply 2001", IEA Solar Heating & Cooling Programme, Feb. 2004.
- (2) Klein, S.A. et al., "TRNSYS 14.2", University of Wisconsin Solar Energy Laboratory, 1996.
- (3) Shah, L.J., Furbo, S., "Modelling Shadows on Evacuated Tubular Collectors with Cylindrical Absorbers", *Journal of Solar Energy Engineering*, Transactions of the ASME, 2005 (In press).
- (4) Gordon J. (ed.). Solar Energy. The State of the Art. ISES Position papers. James & James, London. ISBN: 1-902916-23-9, (2001).
- (5) Shah, L.J., Furbo, S., "Utilization of Solar Radiation at High Latitudes with Evacuated Tubular Collectors" NorthSun 2005, Proceedings, In press.
- (6) Kragh J. et al. "Grønlandske vejrdata. Nuuk. Uummannaq" Department of Civil Engineering, Technical University of Denmark, Nov. 2002.

Bilag 3: Solar World Congress 2005 paper: Numerical investigations of an all glass evacuated tubular collector.

NUMERICAL INVESTIGATIONS OF AN ALL GLASS EVACUATED TUBULAR COLLECTOR

Louise Jivan Shah and Simon Furbo
Department of Civil Engineering
Technical University of Denmark
DK-2800 Kgs. Lyngby
Denmark
E-mail: lis@byg.dtu.dk

ABSTRACT

Heat transfer and flow structures inside all glass evacuated tubular collectors for different operating conditions are investigated by means of Computational Fluid Dynamics (CFD). The investigations are based on a collector design with horizontal tubes connected to a vertical manifold channel.

Three different tube lengths varying from 0.59 m to 1.47 m have been modelled with five different inlet mass flow rates varying from 0.05 kg/min to 10 kg/min with a constant inlet temperature of 333 K. Under these operating conditions the results showed that:

- the collector with the shortest tube length achieved the highest efficiency
- the optimal inlet flow rate was around 0.4-1 kg/min
- the flow structures in the glass tubes were relatively uninfluenced by the inlet flow rate

Generally, the results showed only small variations in the efficiencies. This indicates that the collector design is well working for most operating conditions.

1 INTRODUCTION

All glass evacuated tubular collectors are widely used on the world market. All glass evacuated tubular collectors are based on double glass tubes where the outside of the inner glass wall is treated with an absorbing selective coating and the evacuated space is between the tubes as illustrated in Fig. 1.

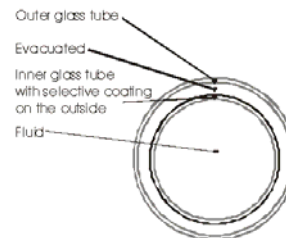


Fig. 1: Design of an all glass evacuated tube.

A collector design based on horizontal tubes connected to a manifold pipe is especially popular due to its low cost. An illustration of the collector design is shown in Fig. 2.

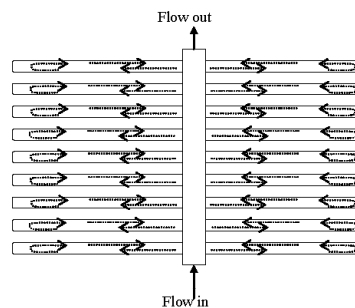


Fig. 2: Illustration of an all glass evacuated tubular collector with horizontal tubes.

The collector fluid enters the bottom of the square manifold channel and leaves at the top of the manifold channel. The intended flow inside the glass tubes is indicated with the arrows. The flow is primarily naturally driven, as the walls of the tubes are hot due to

the solar radiation. However it is unclear, how the operating conditions and the collector geometry influence the flow structures in the tubes and thus the collector performance.

The objective of this work is to investigate the heat transfer and the flow structures inside the tubes for different flow rates and collector geometries by means of Computational Fluid Dynamics (CFD).

2 NUMERICAL INVESTIGATIONS

To solve the flow and energy equations in the glass tubes, a simulation model of the flow in the tubes is developed using the CFD code Fluent 6.1 (1). As illustrated in Fig. 3, only one section of the collector with two horizontal tubes placed in a vertical plane is investigated.

Steady state numerical solutions are obtained for laminar flow with the Boussinesq approximation for buoyancy modelling. The velocity-pressure coupling is treated by using the SIMPLE algorithm and the First Order Upwind scheme is used for the momentum and energy terms.

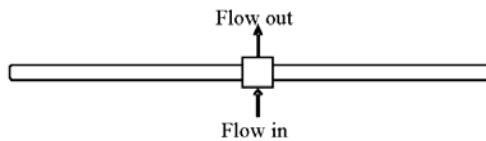


Fig. 3: Illustration of an all glass evacuated tubular collector with horizontal tubes.

2.1 Geometry

The model consists of the inner boundaries of the geometry. The outer glass tube, the evacuated space between the two glass tubes and the wall thickness of the inner glass tube are not included in the model. Also the outer casing and the insulation material of the manifold channel are not included in the model. This means that no solids are simulated – only the fluid is included in the model. The conduction in the inner glass wall is however included in the model. The geometry is summarized in Table 1.

The computational mesh is constructed in the pre-processing program Gambit 2.0.4 (2). The number of computational cells depends on the length of the tubes and is given in Table 1.

Fig. 4 shows a close up of the mesh near the manifold channel.

TABLE 1: GEOMETRY OF THE NUMERICAL MODELS.

Side length of manifold channel:	0.06 m
Glass tube inner diameter:	0.037 m
Glass tube outer diameter (used in manifold channel):	0.047 m
Length of glass tube exposed to solar radiation:	0.59 m 1.17 m 1.47 m
Number of computational cells:	428682 738708 948499
Illustration of geometry:	

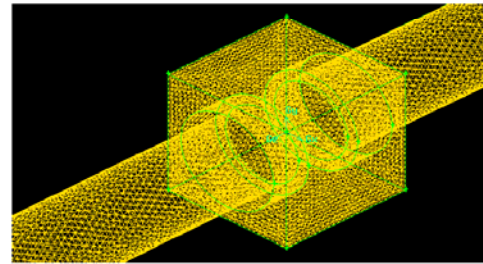


Fig. 4: The mesh near the square manifold channel.

2.2 Boundary conditions

The solar irradiance is simulated as a distributed heat flux on the tube wall. The flux varies from 0 W/m² to 1150 W/m² as shown in Fig. 5. The average flux on the tube wall is 566 W/m².

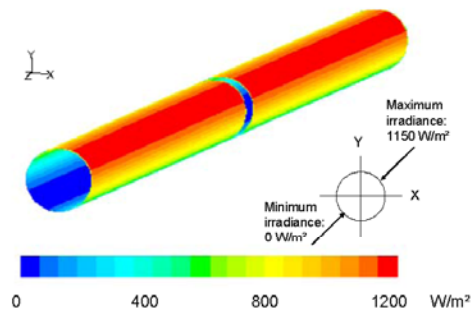


Fig. 5: Distribution of the heat flux on the inner glass tubes.

The heat loss from the tubes is modelled with a heat loss coefficient of $0.85 \text{ W/m}^2\text{K}$ (3) and a constant ambient temperature of 293 K . The heat loss coefficient is related to the absorber area. The manifold channel is assumed to have zero heat loss.

Five different inlet mass flow rates of respectively 0.05 kg/min , 0.4 kg/min , 1 kg/min , 3 kg/min and 10 kg/min have been computed.

The inlet velocity profile has been found by first making a computation with a uniform inlet velocity profile. The outlet velocity profile from this simulation has then been used as the inlet velocity profile for the final simulation.

The inlet temperature has been 333 K during all computations. A 40% propylene-glycol/water mixture has been used as working fluid.

3 RESULTS

The presented results will include illustrations of flow patterns in the vertical centre plane of the model near the manifold channel and in the manifold outlet plane. Further, some overall analyses of the “collector” performance as a function of tube lengths and mass flow rates will be presented.

3.1 Flow distribution

For a tube length of 1.17 m , the left column in Fig. 6 shows velocity vectors in the vertical tube centre plane near the manifold channel for the five investigated inlet mass flow rates.

At the smallest mass flow rate (top-left picture) it can be seen how the fluid flows directly from the inlet in the manifold channel out in the two horizontal tubes. The fluid returns to the manifold channel along the top of the tubes. The two flows from the two tubes exits at the outlet with a profile, which is clearly formed by the flows in the tubes.

The flow patterns for the next two flow rates look similar to the flow pattern for the lowest flow rate; however, there is one significant difference. Due to the larger inlet velocities, the flow rises higher in the manifold channel before it, due to buoyancy forces, turns down to the tube bottom wall and flows out in the tubes. The differences in the forced- and buoyancy driven flows are evident just by seeing how far up in the manifold tube the flow rises.

For the two highest flow rates it is clear that some of the flow passes directly through the manifold channel without entering the tubes. Therefore, the outlet velocity profiles look different for the highest flow rates

compared to the outlet velocity profiles for the lowest flow rates.

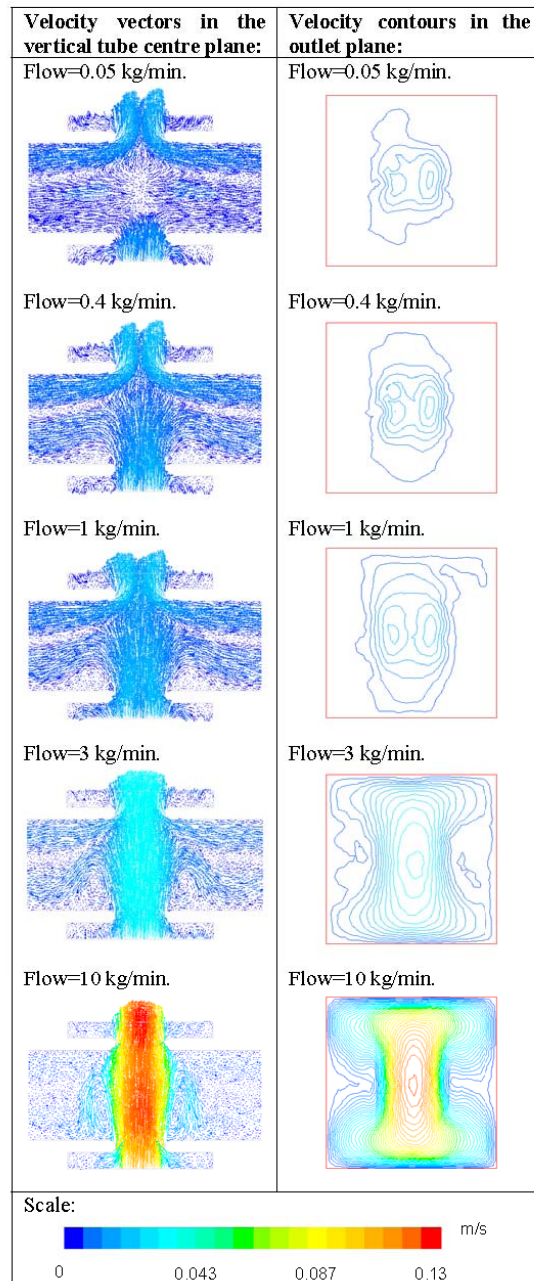


Fig. 6: Velocity patterns in the vertical tube centre plane (left column) and in the outlet plane (right column). Tube length: $L=1.17 \text{ m}$.

The right column in Fig. 6 shows the velocity contours in the outlet plane. It can be seen how the velocity pattern changes from being dominated by the two flows from the tubes for the lowest inlet flow rates to, for the highest flow rates, being dominated mainly by the inlet flow.

3.2 Thermal performance

The thermal performance is investigated by calculating efficiencies for the different combinations of flow rates and tube lengths. The efficiency, η , is defined as the ratio between the power out of the collector, $P_{\text{collector}}$, and the distributed heat flux absorbed by the collector, P_{solar} :

$$\eta = \frac{P_{\text{collector}}}{P_{\text{solar}}}$$

Notice that this efficiency cannot be compared with the traditional way of defining the collector efficiency as optical losses are not included in the efficiency used here.

Fig. 7 shows the efficiency as a function of the mass flow rate. The efficiency is highest for flow rates around 0.4 kg/min – 1 kg/min. The explanation for this result can be found in Fig. 8, which shows the mean temperature in the collector as a function of the mass flow rate. For the largest inlet flow rates (3 kg/min – 10 kg/min) a large part of the fluid flows directly through the manifold channel leaving only a smaller part flowing out in the tubes. Therefore, the average temperature in the whole collector rises. This leads to a higher heat loss and thus a lower efficiency. For the lowest flow rate (0.05 kg/min) almost all the inlet flow goes out in the tubes, but now the flow is so small that this alone leads to an increased average temperature in the whole collector.

That the efficiency in fact decreases with increasing average temperatures in the whole collector is very clear in Fig. 9. Here each dot represents an efficiency found at a given inlet flow rate. All the dots together form an almost straight line with a tilt that shows how the efficiency decreases with increasing heat loss caused by increasing average temperatures in the whole collector. The collector with the shortest tube has the highest efficiency and vice versa.

Finally, Fig. 10 shows the efficiency as a function of the average of the inlet- and outlet temperature. As in Fig. 7 and in Fig. 9 it can be seen that the highest efficiency is achieved for the shortest tube length.

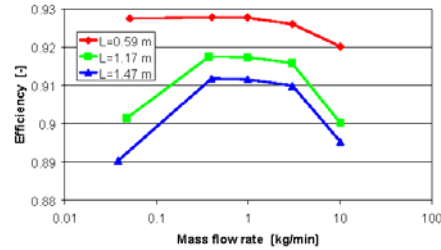


Fig. 7: The efficiency as a function of the mass flow rate.

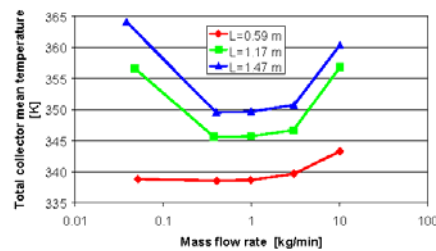


Fig. 8: The mean temperature in the total collector as a function of the mass flow rate.

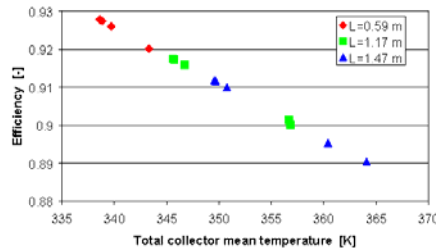


Fig. 9: The efficiency as a function of mean temperature in the whole collector.

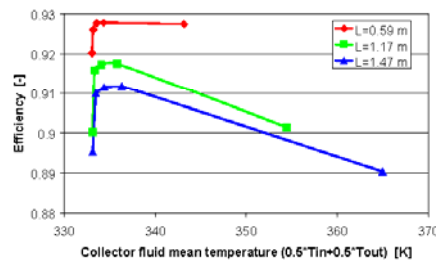


Fig. 10: The efficiency as a function of the average of the inlet- and outlet temperature.

The results further show that the inlet mass flow rate has a relatively small influence (1-2 %) on the resulting efficiencies. This might seem strange considering the large differences in the flow patterns near the manifold channel (Fig. 6). The main reason is that the flow in the tubes at a distance from the manifold channel is relatively unaffected by the inlet flow.

For a tube length of $L=1.17$ m, Fig. 11 shows the maximum velocity magnitude as a function of the distance from the manifold centre. For the varying inlet flows, the figure shows that close to the manifold channel there are differences in the maximum velocity magnitude but further out in the tubes there are almost no differences in the maximum velocity magnitude. This explains why the absolute differences in the collector efficiencies are so small for the varying inlet flow conditions. Fig. 11 also shows that the flows out in the tubes are:

- largest for an inlet flow of 0.4 kg/min
- 2nd largest for an inlet flow of 1 kg/min
- 3rd largest for an inlet flow of 3 kg/min
- 2nd smallest for an inlet flow of 0.05 kg/min and
- smallest for an inlet flow of 10 kg/min

This corresponds nicely with the results presented in Fig. 7 where the order of efficiencies is the same.

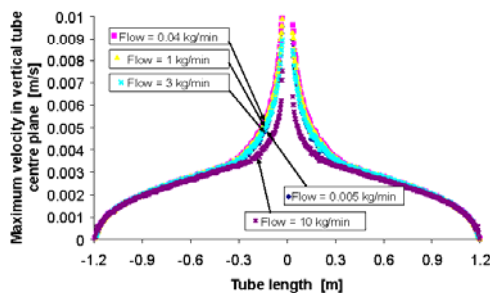


Fig. 11: Maximum velocity magnitude in the tubes (outside the manifold channel) in the vertical centre plane.

Finally, it should be mentioned that another reason for the small differences in the calculated efficiencies is that the heat loss coefficient for the tubes is very small. Due this low heat loss coefficient, the differences in the mean temperature in the whole collector have an only minor influence on the final efficiency.

4 CONCLUSIONS

The objective of this work was to investigate the heat transfer and the flow structures inside all glass

evacuated tubular collectors for different operating conditions by means of CFD.

A collector design based on horizontal tubes connected to a manifold channel has been investigated. The working principle of the collector is that the collector fluid enters the bottom of the square manifold channel, circulates in the glass tubes and leaves at the top of the manifold channel.

Three different tube lengths of 0.59 m, 1.17 m and 1.47 m have been modelled with five different inlet mass flow rates of respectively 0.05 kg/min, 0.4 kg/min, 1 kg/min, 3 kg/min and 10 kg/min. The inlet temperature has been 333 K during all computations and a 40% propylene-glycol/water mixture has been used as the collector fluid. The average solar radiation absorbed on the tube wall has been 566 W/m².

Under these operating conditions the results showed that:

- the collector with the shortest tube length achieved the highest efficiency
- the optimal inlet flow rate was around 0.4-1 kg/min
- the flow structures in the glass tubes were relatively uninfluenced by the inlet flow rate

All the results were directly related to the resulting average temperature in the whole collector. The shortest tube length gave the lowest average temperature. The optimal inlet flow rate was around 0.4-1 kg/min as larger inlet flow rates (3 kg/min – 10 kg/min) gave a larger part of the fluid flowing directly through the manifold channel leaving only a smaller part flowing out in the tubes. Therefore, the average temperature in the whole collector rose. For the lowest flow rate (0.05 kg/min) almost all the inlet flow went out in the tubes, but here the flow was so small that this alone lead to an increased average temperature in the whole collector.

Generally, the results showed only small variations in the efficiencies. This indicates that the collector design is well working for most operating conditions.

5 NOMENCLATURE

η	collector efficiency	[-]
$P_{\text{collector}}$	Power from collector	[W]
P_{solar}	Radiation absorbed by the collector	[W]
L	Tube length	[m]

6 ACKNOWLEDGEMENTS


This study is financed by the VILLUM KANN RASMUSSEN FOUNDATION.

7 REFERENCES

- (1) Fluent 6.1 User's Guide (2003). Fluent Inc. Centerra Resource Park 10 Cavendish Court Lebanon, NH 03766
- (2) Gambit 2 User's Guide (2001). Fluent Inc. Centerra Resource Park 10 Cavendish Court Lebanon, NH 03766
- (3) Qin I. and Furbo S. (1999) *Vakuumsølsfangere fra Kina*. Report R-032. Department of Buildings and Energy, Technical University of Denmark.

Bilag 4: North Sun 2005 Congress præsentation: Utilization of solar radiation at high latitude with evacuated tubular collectors.

BYG·DTU
 Department of Civil Engineering




Utilization of Solar Radiation

at High Latitudes with

Evacuated Tubular Collectors

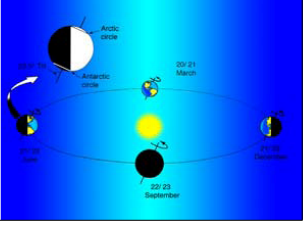
Louise Jivan Shah
 Department of Civil Engineering
 Technical University of Denmark
 Building 118, DK-2800 Kgs. Lyngby
 DENMARK
 E-mail: ljs@byg.dtu.dk

BYG·DTU
 Department of Civil Engineering

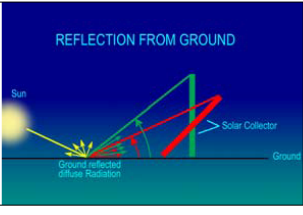


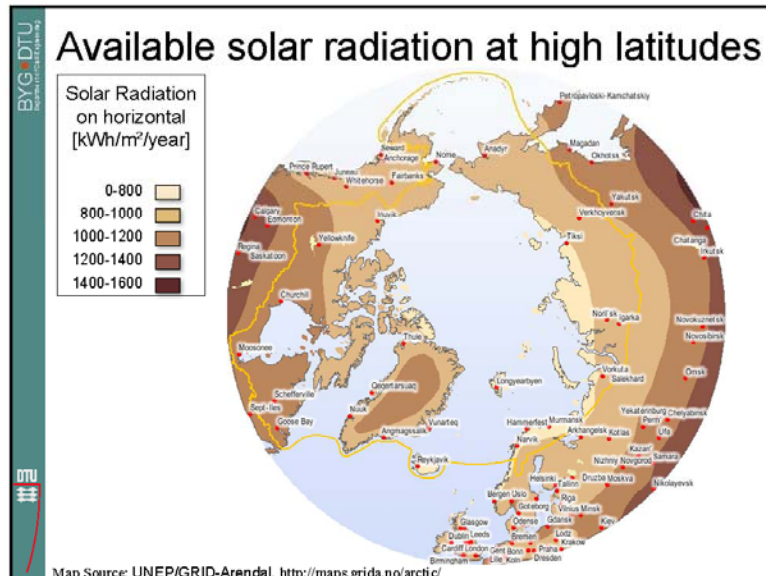
Solar energy at high latitudes

- Large season variations
- Solar radiation from all directions



- High ground reflections due to snow
- Low ambient temperatures





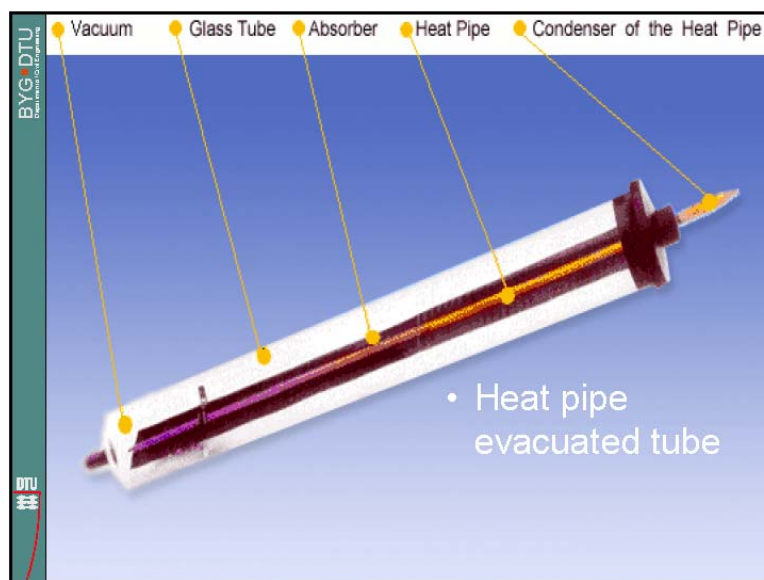
Solar collectors for northern latitudes

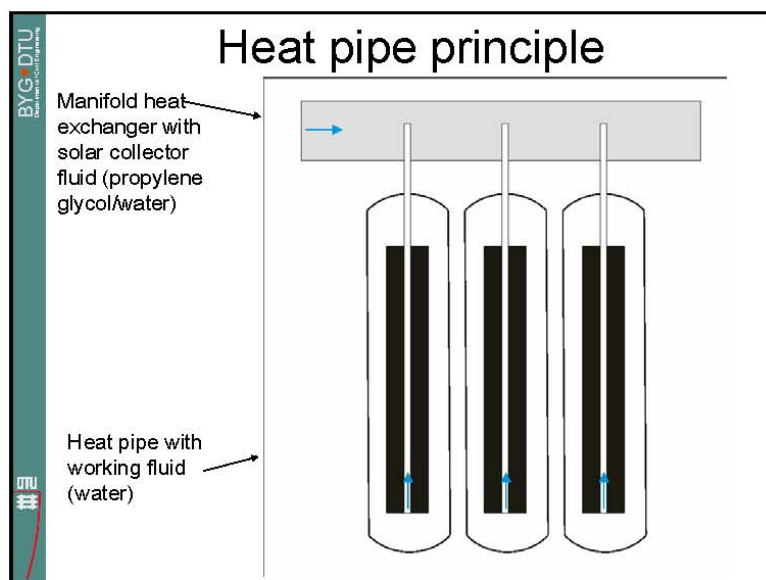
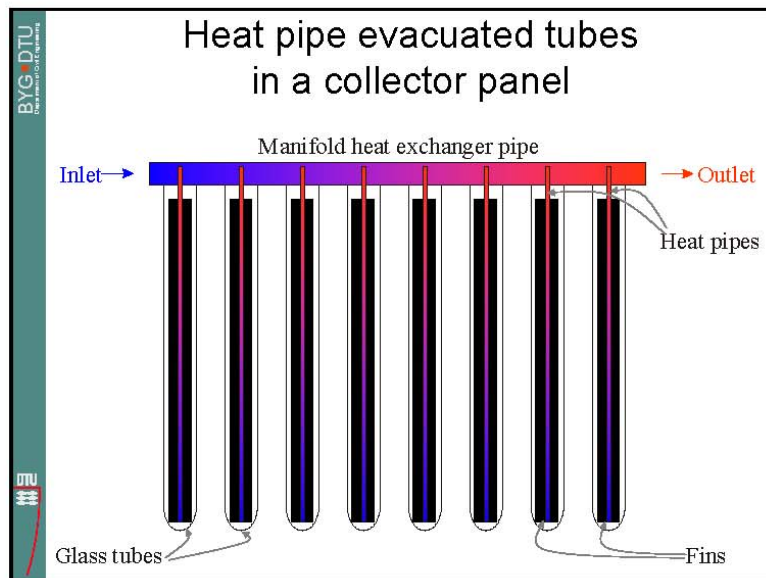
- When solar collectors are developed for high latitudes, it is an advantage if the collectors:
 - ☺ Can utilize solar radiation from all directions
 - ☺ Have a low heat loss (due to low ambient temperatures)
 - ☺ Utilize ground reflected radiation well (due to large ground reflection coefficient)

BYG-DTU
TECHNICAL UNIVERSITY OF DENMARK

Evacuated tubular collectors

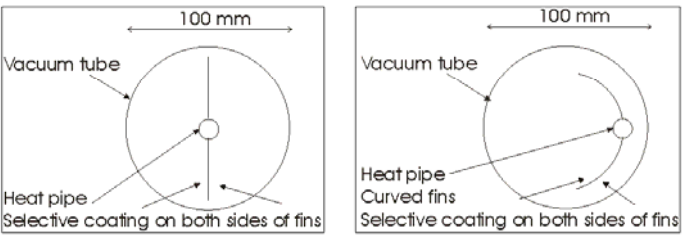
- ☺ Low heat loss coefficient
 - Vacuum insulation
- ☺ High efficiency
 - Due to low heat loss
- ☺ Utilize solar radiation from all directions
 - Double-sided absorbers with coating on both sides
- ☺ Mass produced in China
 - Low cost





BYG-DTU
Building Research
Technical University of Denmark

Heat pipe evacuated tubular collectors with **double-sided absorbers**



100 mm

Vacuum tube

Heat pipe

Selective coating on both sides of fins

100 mm

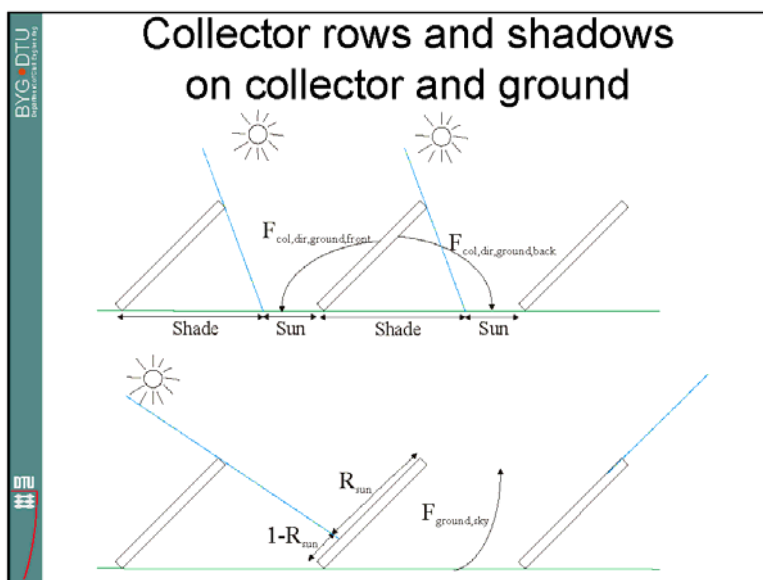
Vacuum tube

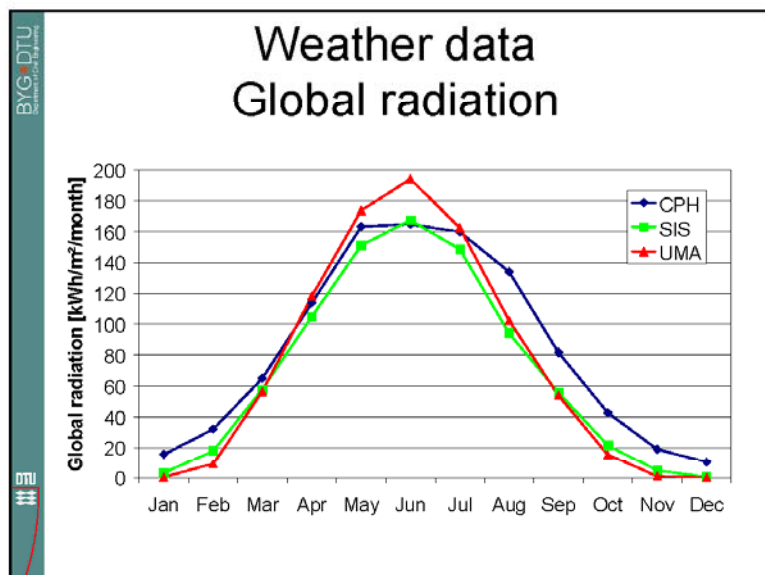
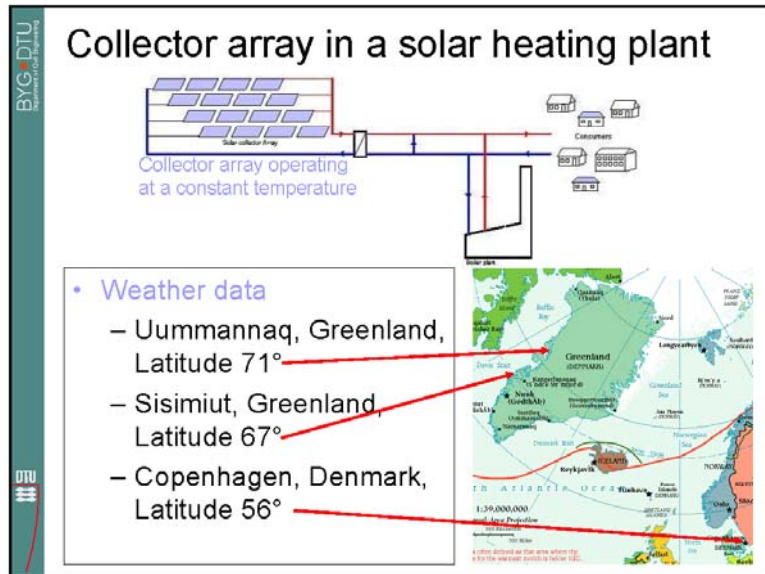
Heat pipe

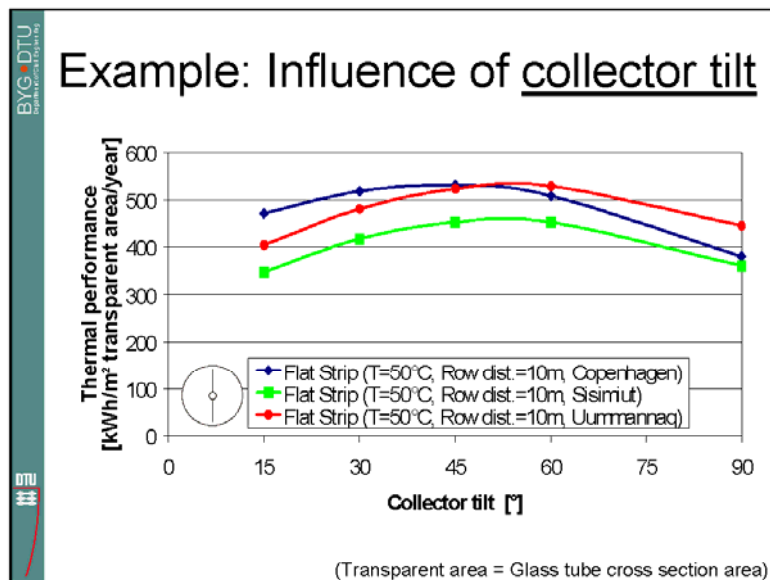
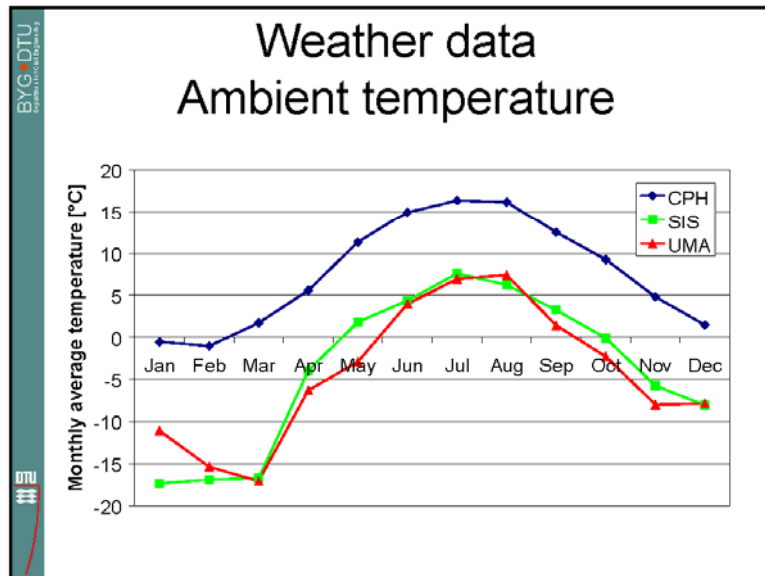
Curved fins

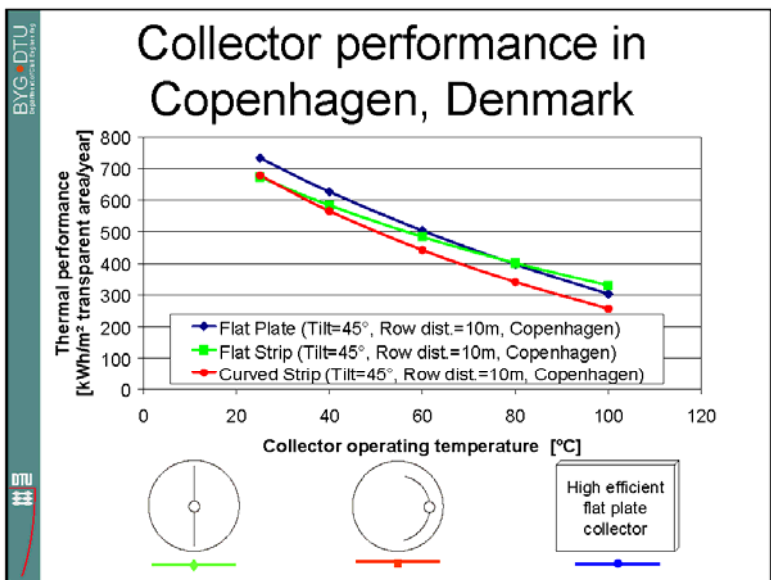
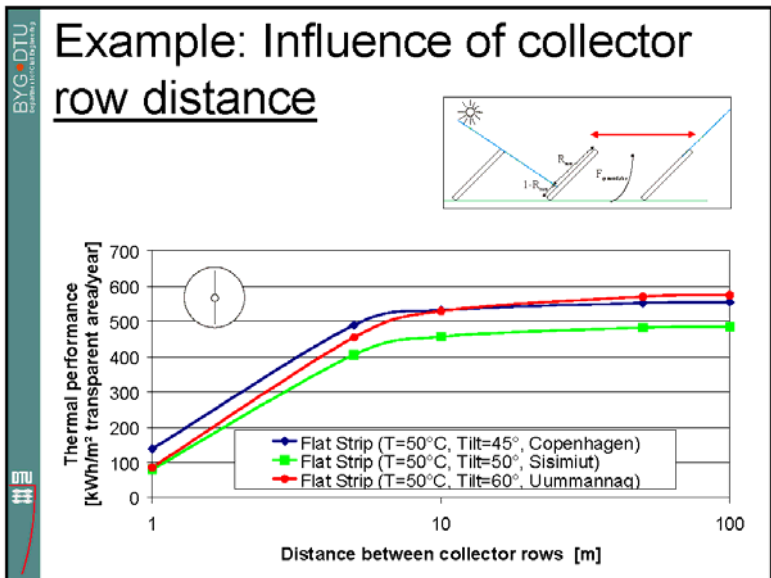
Selective coating on both sides of fins

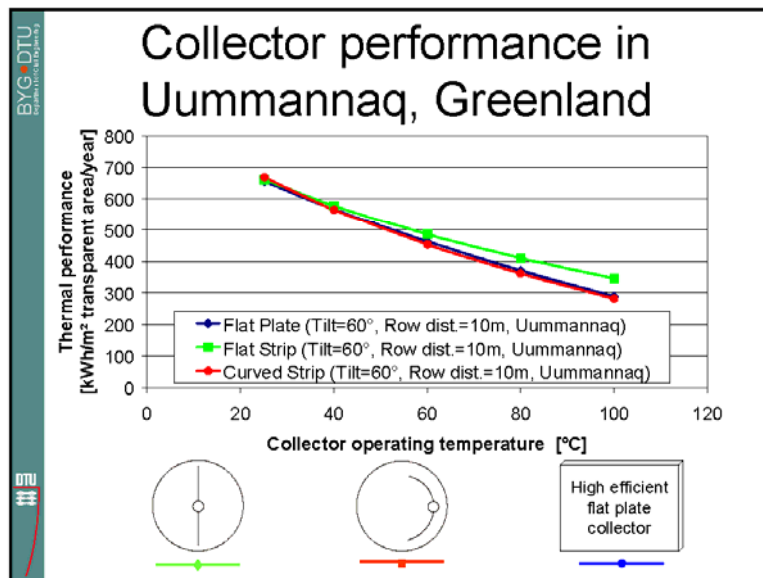
- **Research work:**
 - New collector theory is developed - TrnSys
 - Calculation yearly thermal performance is now possible
 - Detailed optimization of collector design is now possible







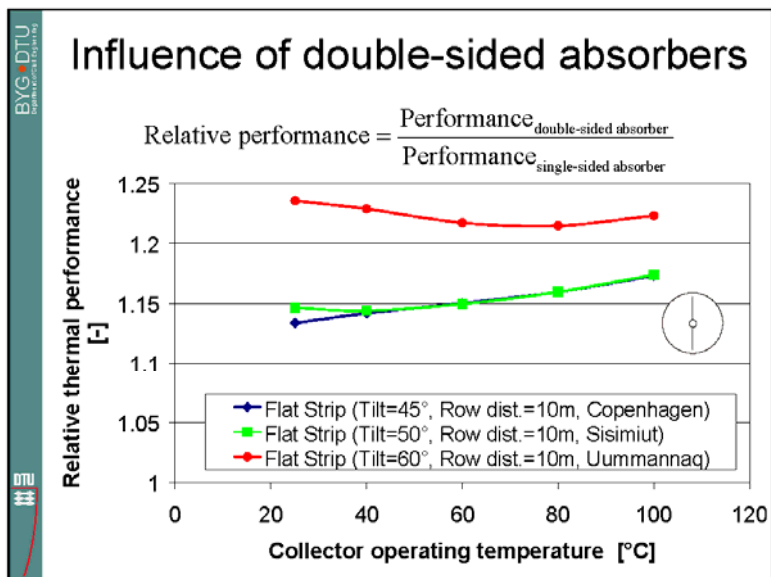
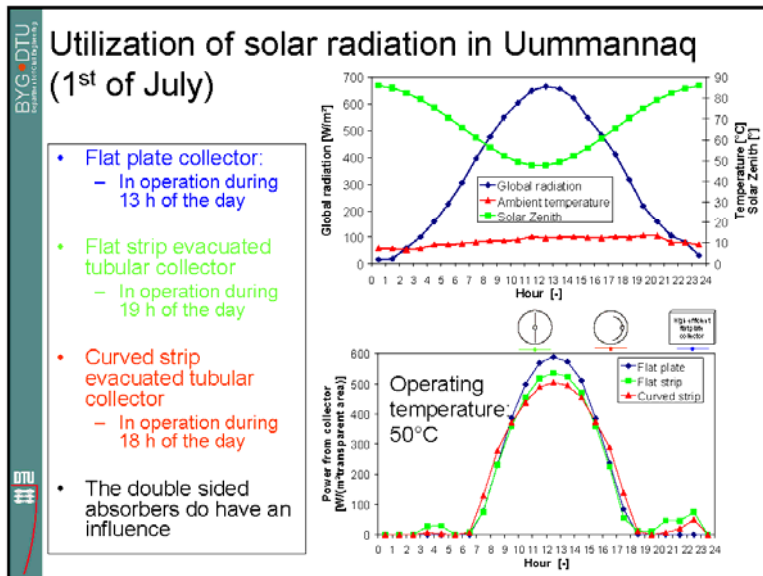




BYG DTU
TECHNICAL UNIVERSITY OF DENMARK

Observations – Collector performance

- Evacuated tubular collectors are relatively better performing in Uummannaq than in Copenhagen, compared to the flat plate collector.
- Does the evacuated tubular collectors with double-sided absorbers have an extra advantage compared to flat plate collectors at high latitudes due to the possibility of utilization of solar radiation from all directions?



BYG DTU
 Department of Building
 Physics




Conclusions

- Compared to a flat plate collector, the heat pipe evacuated tubular collectors are relatively better performing in Uummannaq than in Copenhagen
- The influence of the double-sided absorber increases with increasing latitudes.

BYG DTU
 Department of Building
 Physics

Further work

- **Measurements**
 - New test facility
 - Test of 5 differently designed evacuated tubular collectors
 - Direct performance comparison
 - Final validation of theoretical models
- **Optimization work**
- **Design**
 - Based on the findings and on economy considerations, well designed evacuated tubular collectors for Northern latitudes will be recommended



Bilag 5: ISES Solar World Congress præsentation: Theoretical investigations of differently designed heat pipe evacuated tubular collectors.

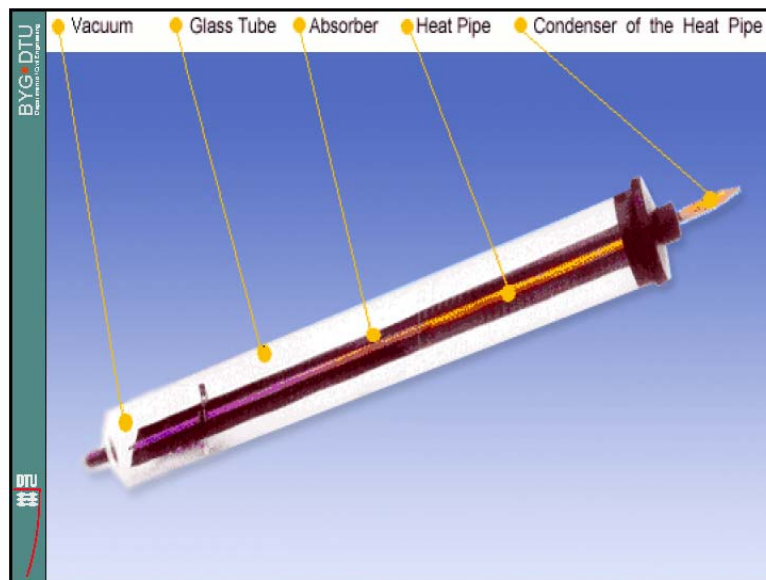
Theoretical Investigations of differently designed Heat Pipe Evacuated Tubular Collectors

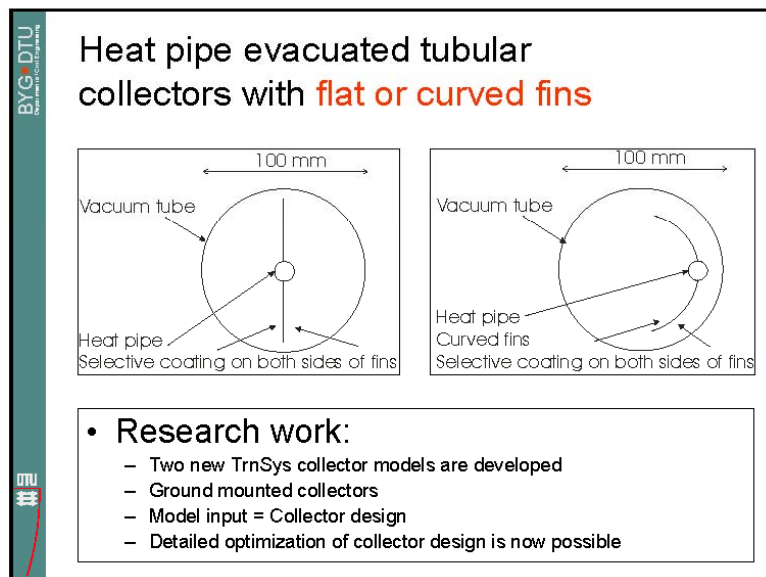
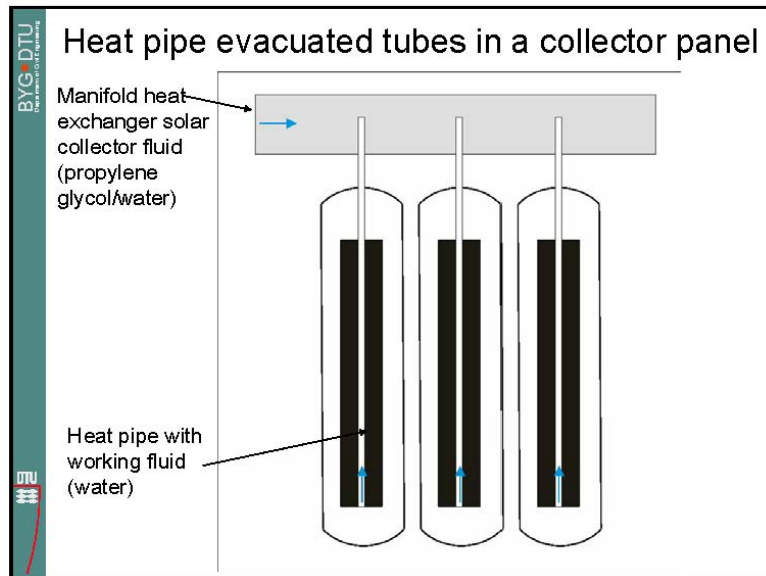
Louise Jivan Shah and Simon Furbo

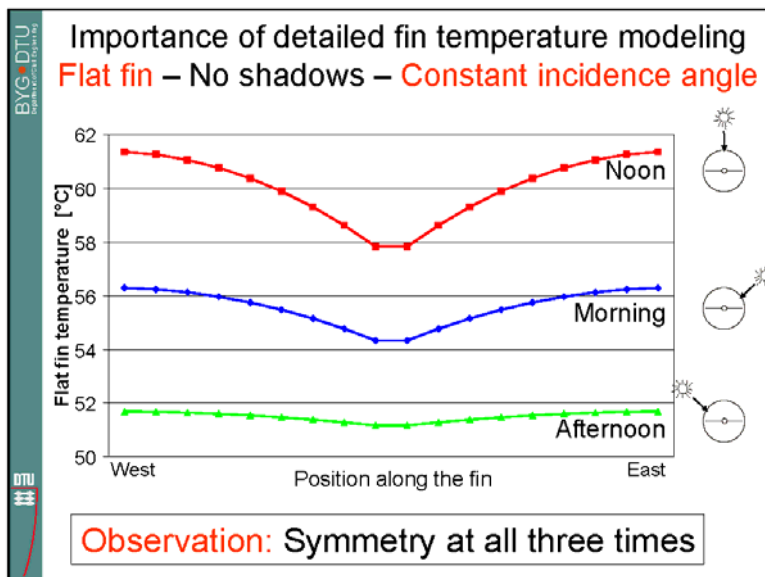
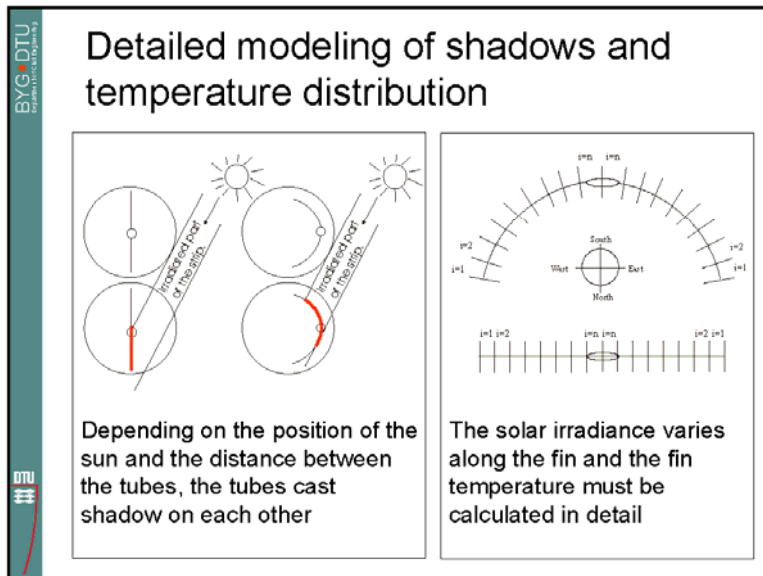
Department of Civil Engineering
Technical University of Denmark

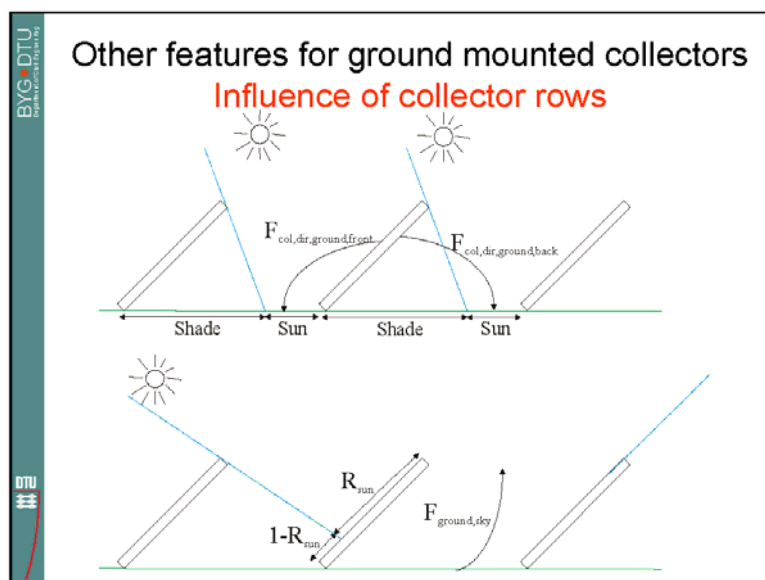
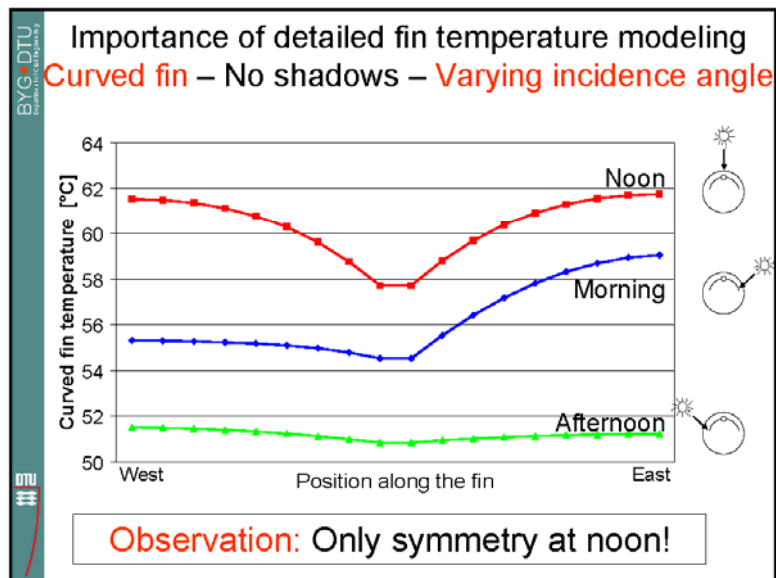
E-mail:

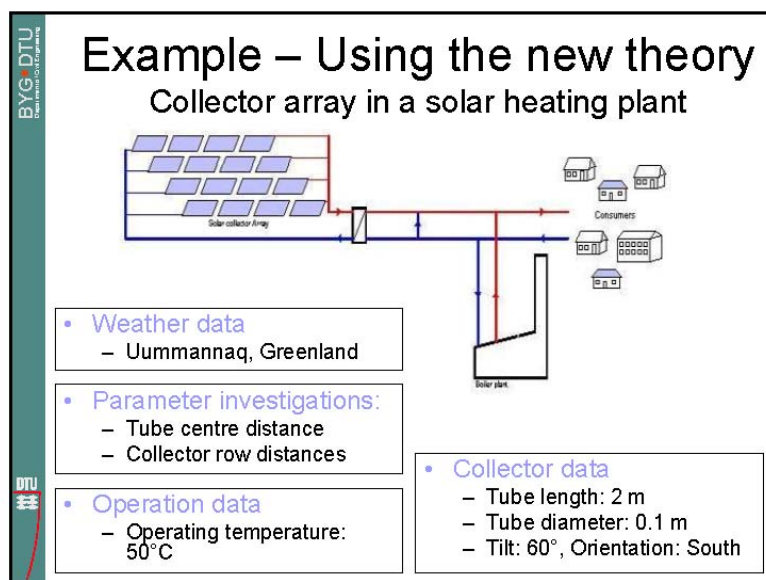
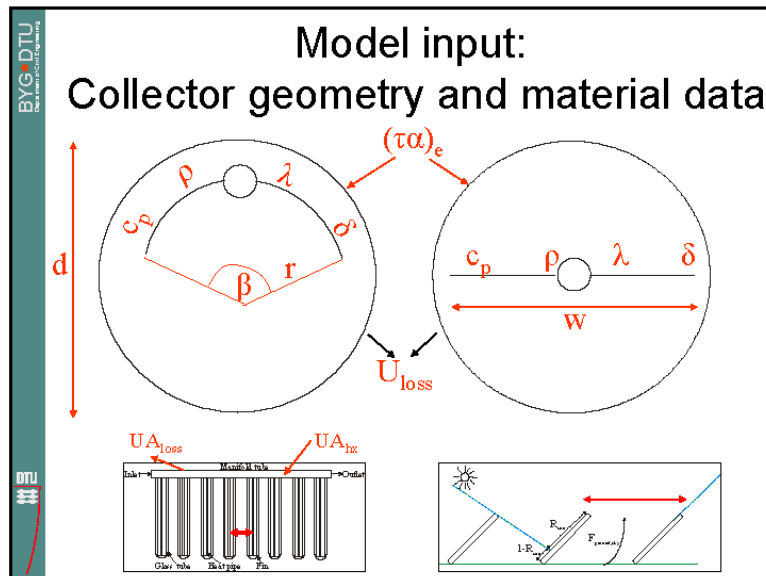
lis@byg.dtu.dk

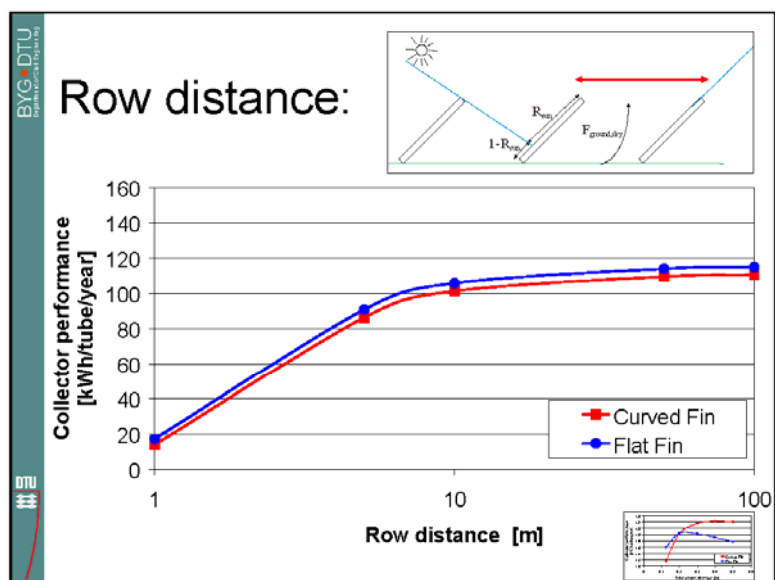
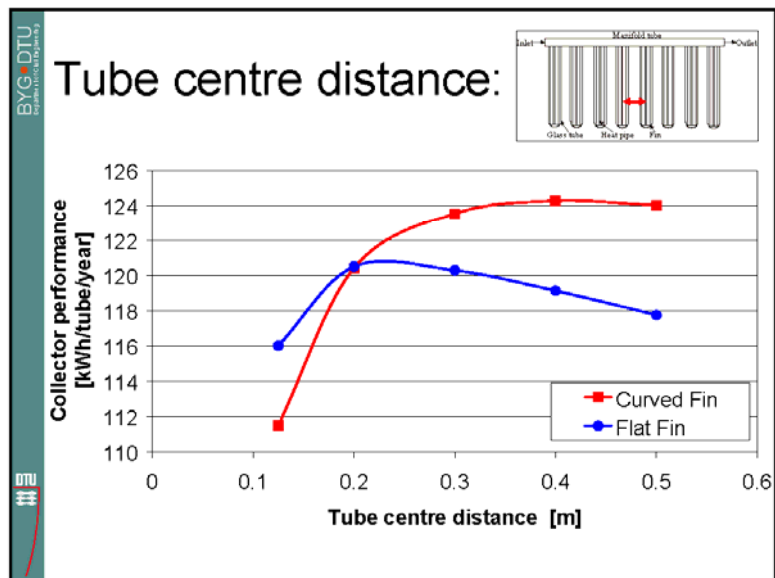









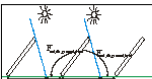

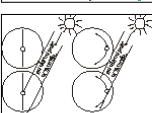
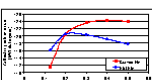




BYG-DTU
DTU

Summary




- Developed two new Trnsys collector types for heat pipes with double sided absorbers
- Detailed view factor modelling
- Detailed shadow modelling
- Detailed fin temperature modelling
- Model input = Exact collector design
- Detailed optimization of collector design is now possible

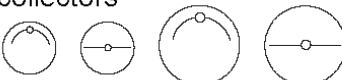






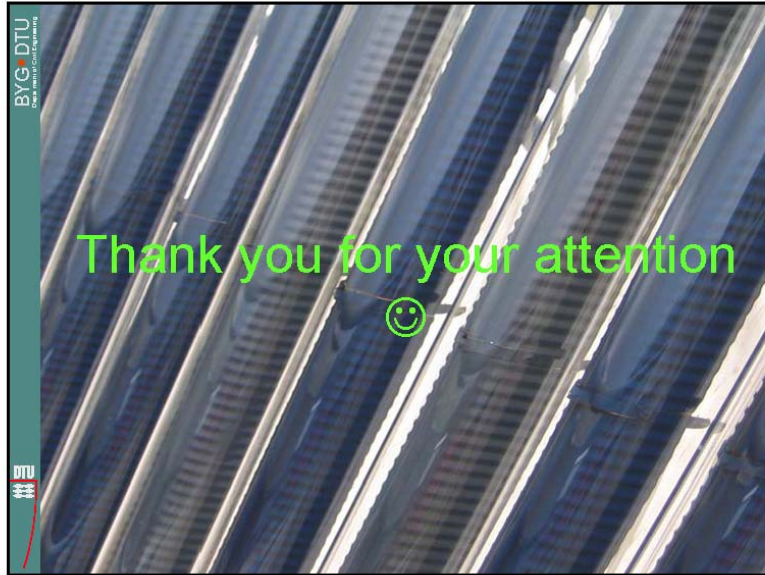
BYG-DTU
DTU

Further work

- Measurements
 - New test facility
 - Test of 4 differently designed heat pipe evacuated tubular collectors
 - Direct performance comparison
 - Final validation of theoretical models





Bilag 6: ISES Solar World Congress præsentation: Theoretical investigations of an all glass evacuated tubular collector.

Numerical Investigations of an All Glass Evacuated Tubular Collector

Louise Jivan Shah and Simon Furbo

Department of Civil Engineering
Technical University of Denmark

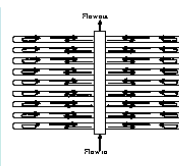
E-mail:

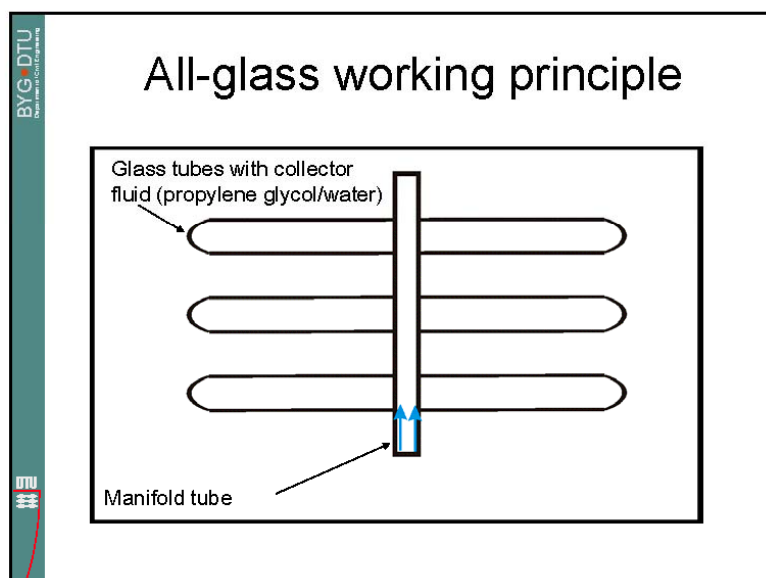
lis@byg.dtu.dk

All-glass evacuated tubular collectors

Investigation of flow and temperature patterns
inside the tubes

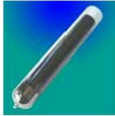
- All-glass collector
- Heat transfer
- Flow structures



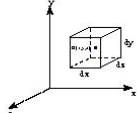


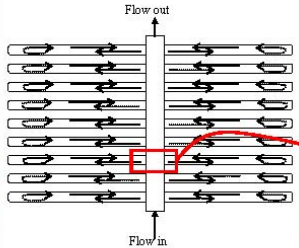
BYG-DTU
 Department of Building Physics

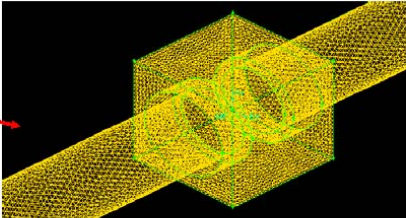
Computational Fluid Dynamics (CFD)



- A grid is made of the geometry and governing equations of fluid flow are solved numerically
- With CFD temperatures and flow patterns are determined









BYG-DTU
 Department of Building Physics

CFD investigations:





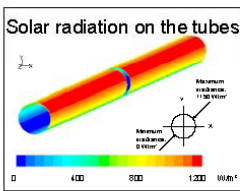
Calculations:

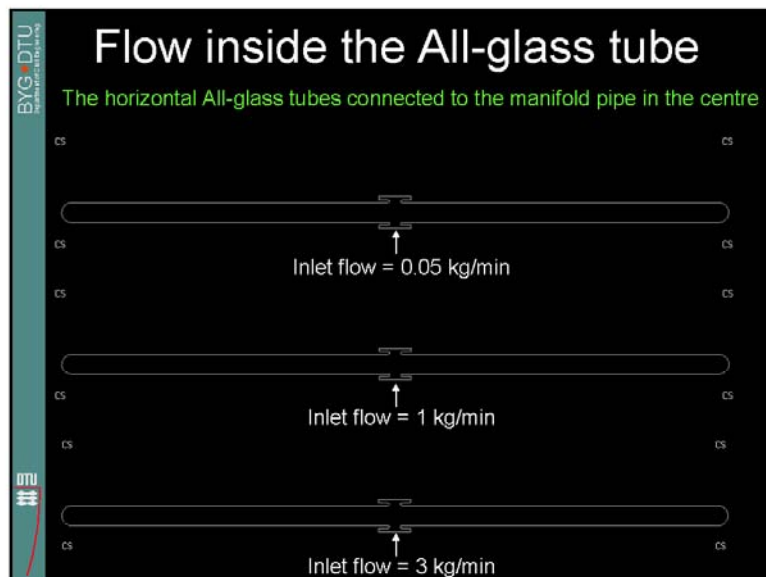
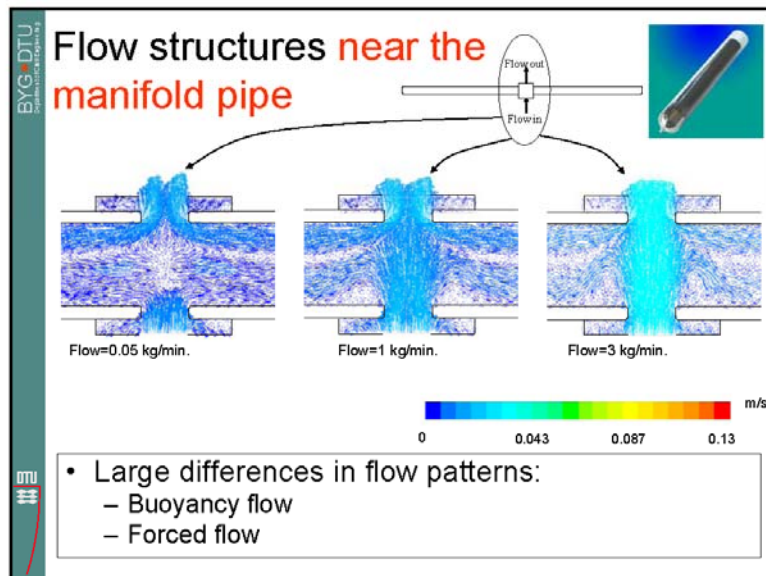
- 5 different inlet flow rates:
 - 0.05 kg/min – 10 kg/min.
 - Realistic inlet velocity pattern
- Inlet temperature: 60 °C
- Uneven solar radiation

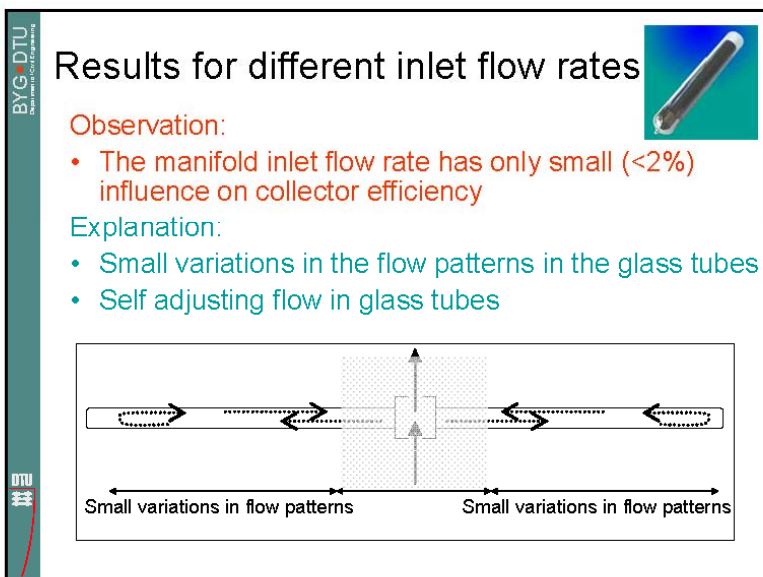
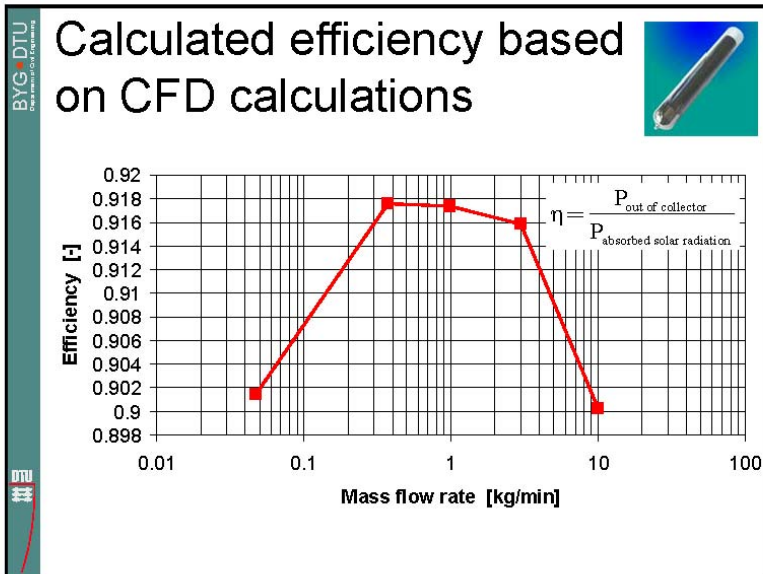
Results:

- Flow structures
- Influence on collector efficiency

Solar radiation on the tubes








BYG-DTU
Department of Building Physics

DTU


Summary




- Example of how Computational Fluid Dynamics gives detailed useful results
- Optimal manifold inlet flow rate is around 0.4-1 kg/min.
- Flow structures in the glass tubes were relatively uninfluenced by the manifold inlet flow rate
- This indicates that the collector design is well working for most operating conditions.

BYG-DTU
Department of Building Physics


DTU




Thank you for your attention



Bilag 7: Præsentation ved Solar seminar ved Beijing Solar Energy Institute, Beijing, Kina: Side-by-side tests of Seido collectors




BYG-DTU
Department of Civil Engineering




DTU

Side-by-side tests of Seido collectors

Louise Jivan Shah
Department of Civil Engineering
Technical University of Denmark
E-mail:
lis@byg.dtu.dk



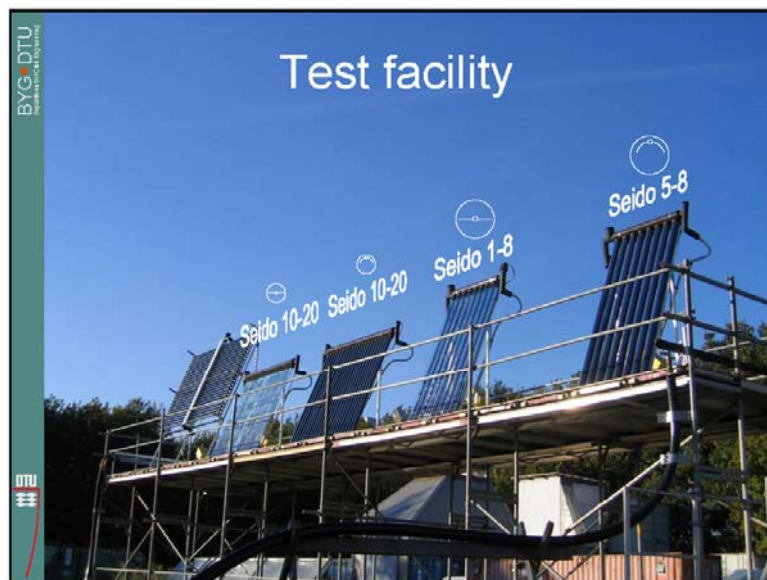
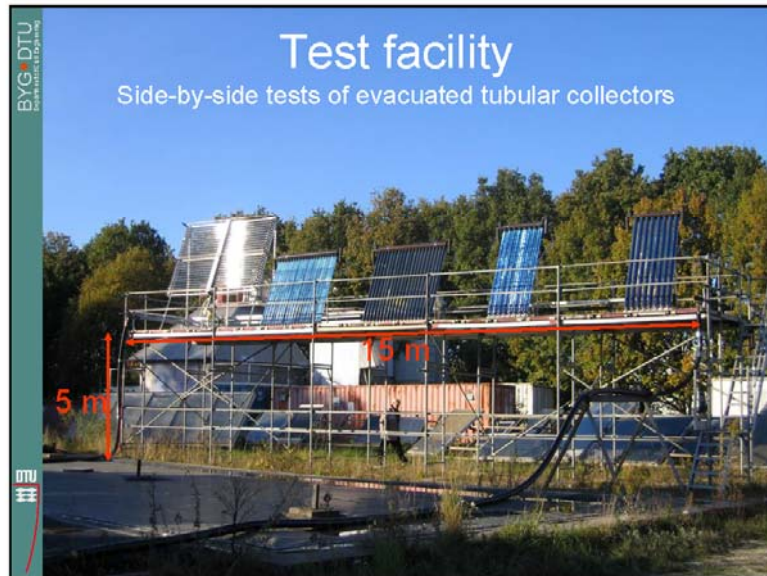
BYG-DTU
Department of Civil Engineering



DTU

Overview

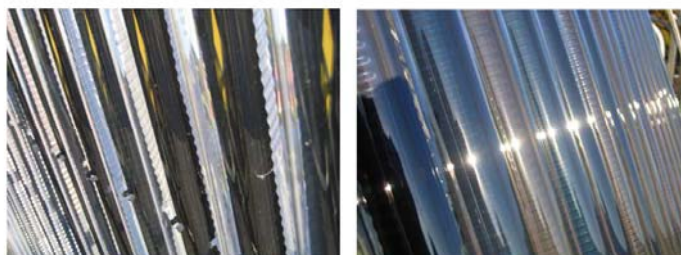
- Test facility
- Measurements
- Simulation models
- Parameter studies
- Conclusion





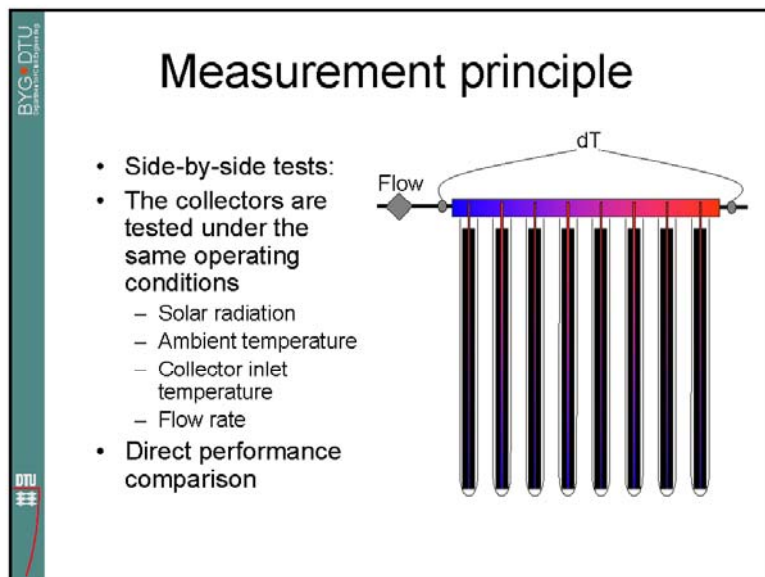
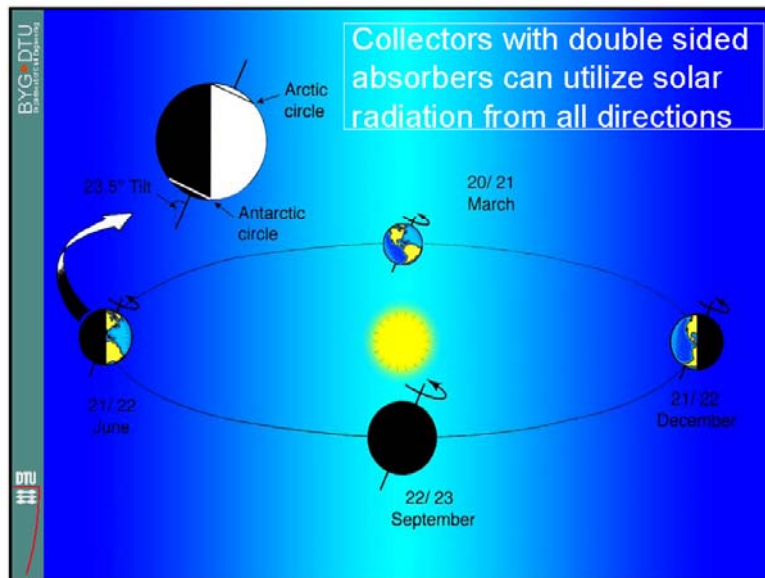
Double-sided absorbers

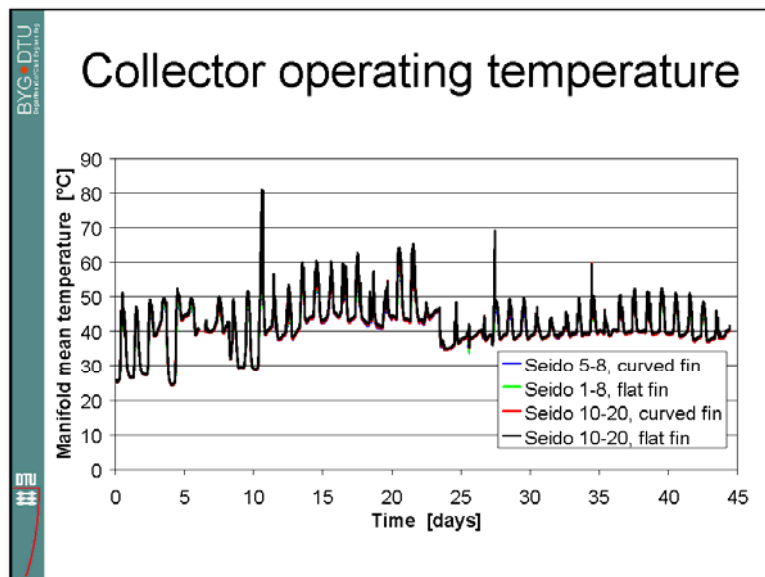
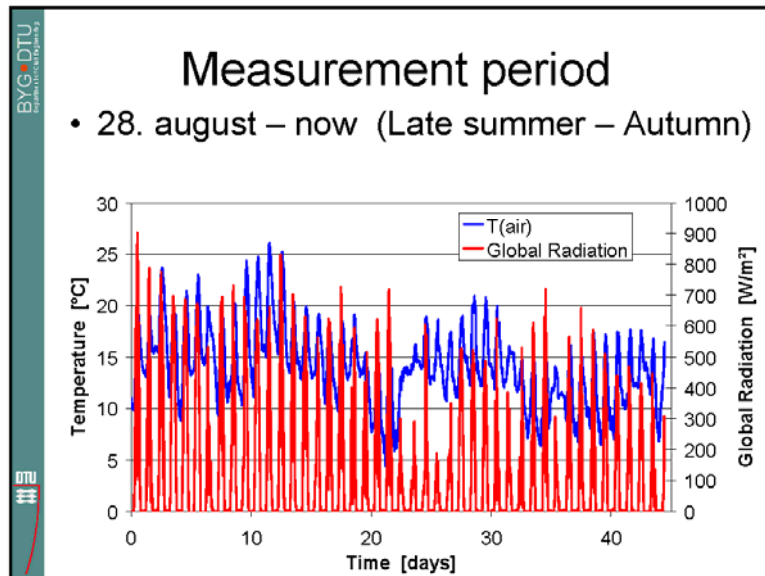
- Absorber coating on both sides of the fin

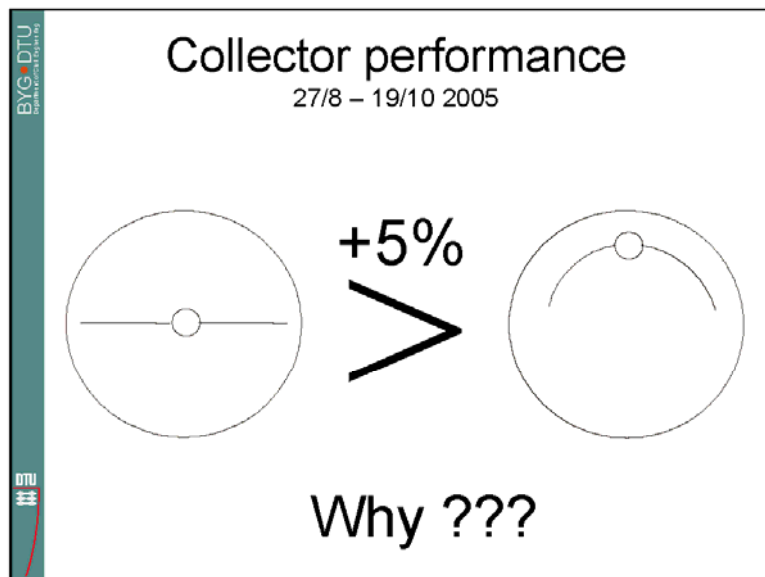
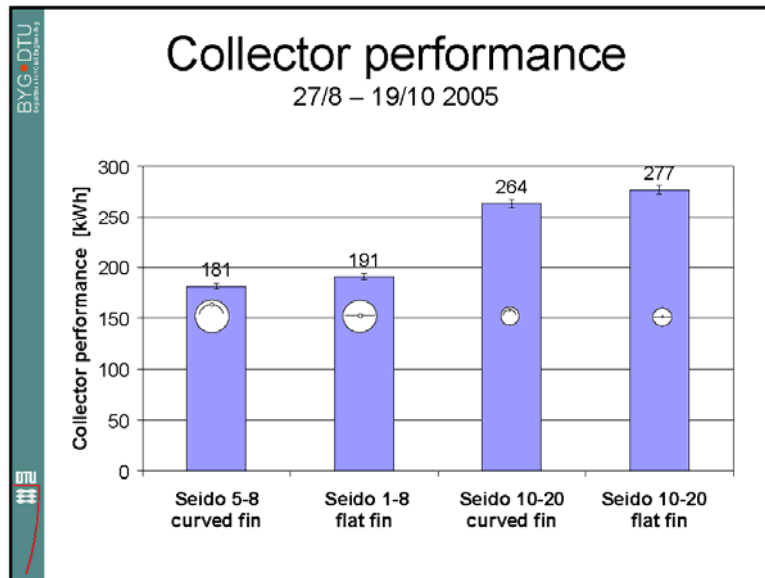


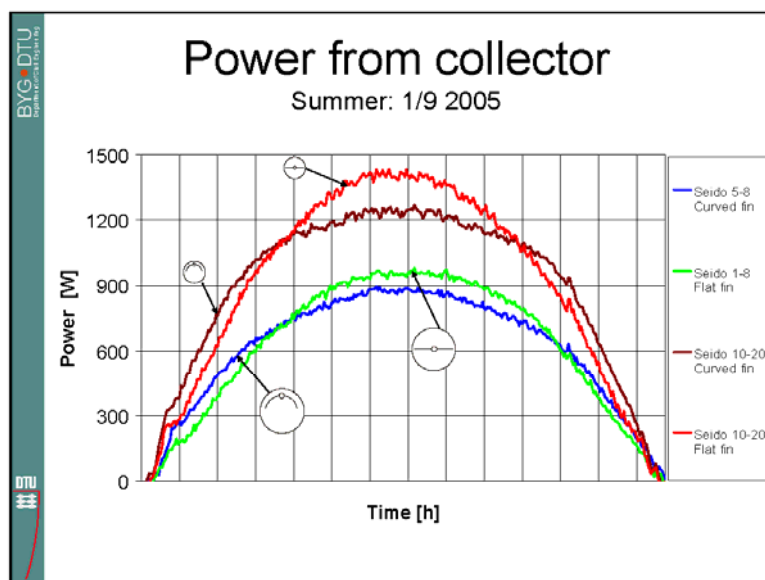
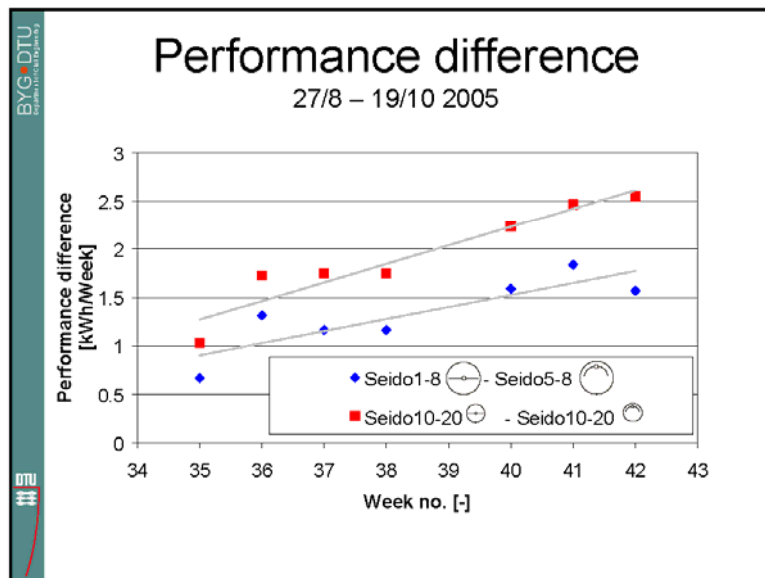
Back side

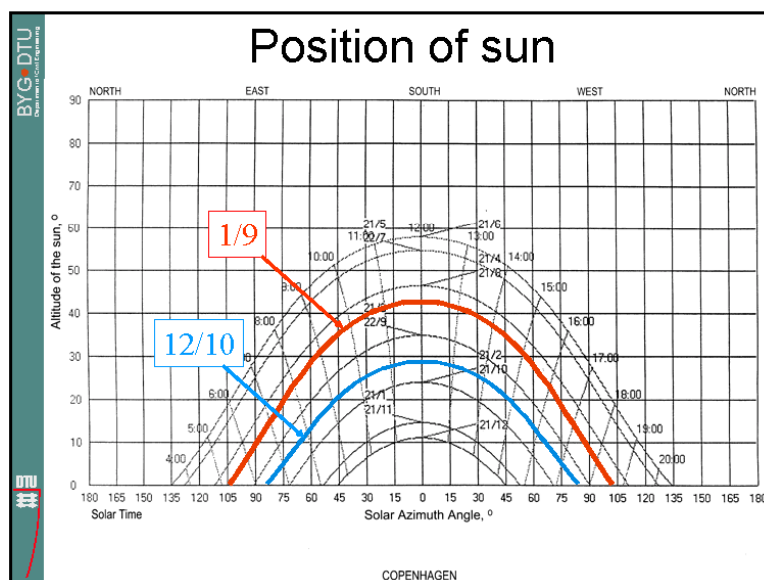
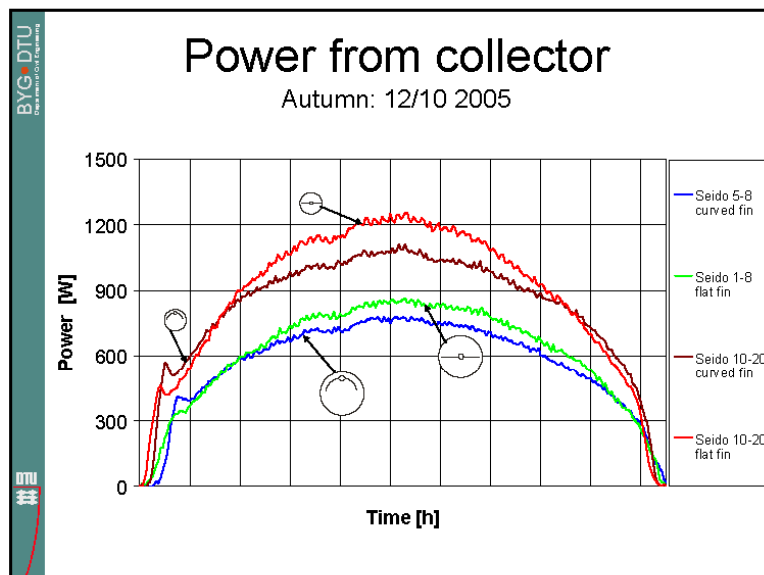
Front side


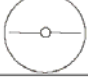

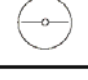








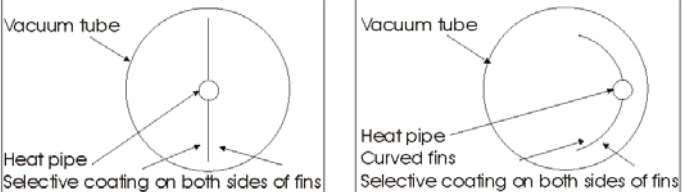


BYG-DTU Department of Building Physics		
Manifold heat loss coefficient		
Seido 5-8	0.4 W/K	
Seido 1-8	0.6 W/K	
Seido 10-20	0.8 W/K	
Seido 10-20	1.1 W/K	
DTU		

BYG-DTU Department of Building Physics	
Preliminary conclusions from measurements	
<ul style="list-style-type: none"> • All collectors were easily installed and operate without any problems • The flat fin collectors perform better than the curved fin collectors <ul style="list-style-type: none"> – Less significant during summertime – Main reason is due to different effective incidence angles • There are significant differences in the manifold heat loss coefficients <ul style="list-style-type: none"> – The manifold pipes for the flat fin collectors have higher heat losses than the manifold pipes for the curved fin collectors 	
DTU	

BYG DTU
Department of Building Physics

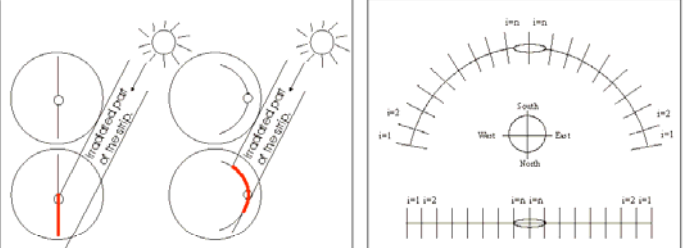
Theoretical work



- Research work:
 - Two new TrnSys collector models are developed
 - Model input = Collector design
 - Detailed optimization of collector design is now possible

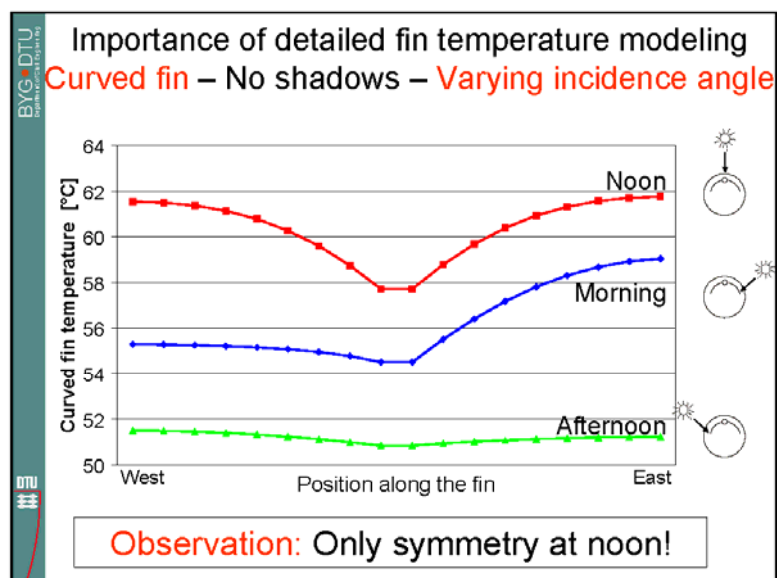
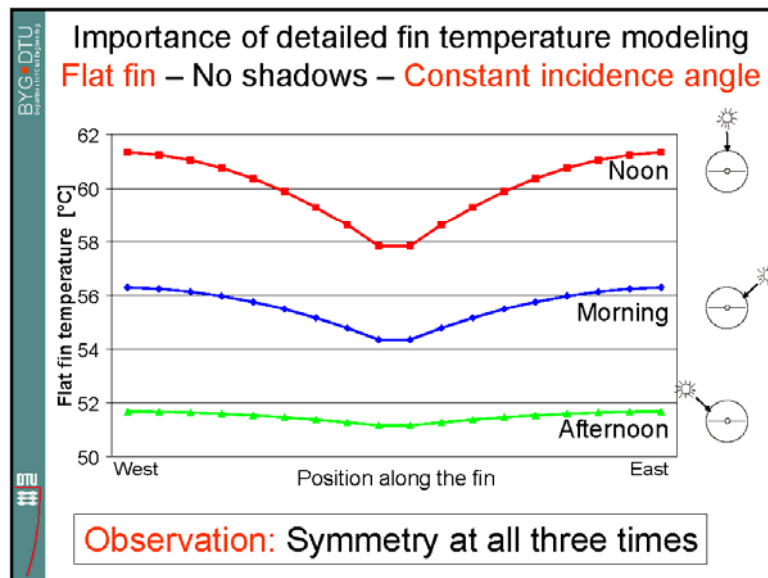
BYG DTU
Department of Building Physics

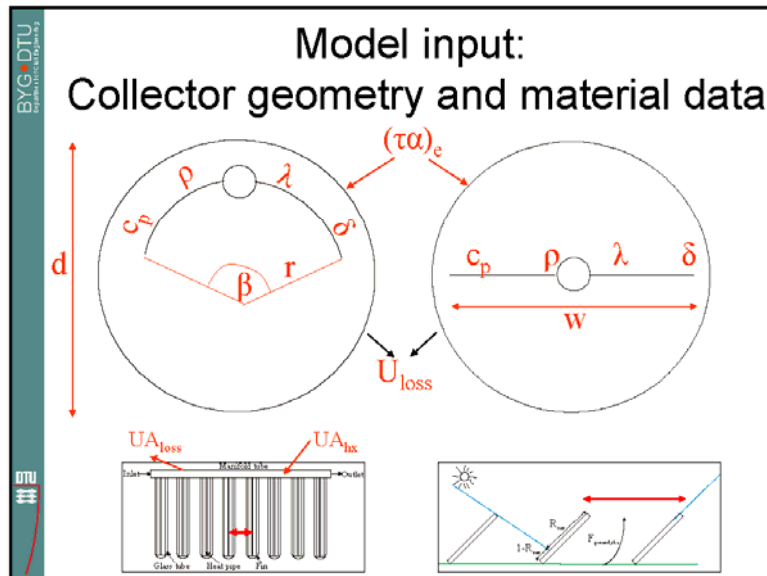
Detailed modeling of shadows and temperature distribution



Depending on the position of the sun and the distance between the tubes, the tubes cast shadow on each other

The solar irradiance varies along the fin and the fin temperature must be calculated in detail



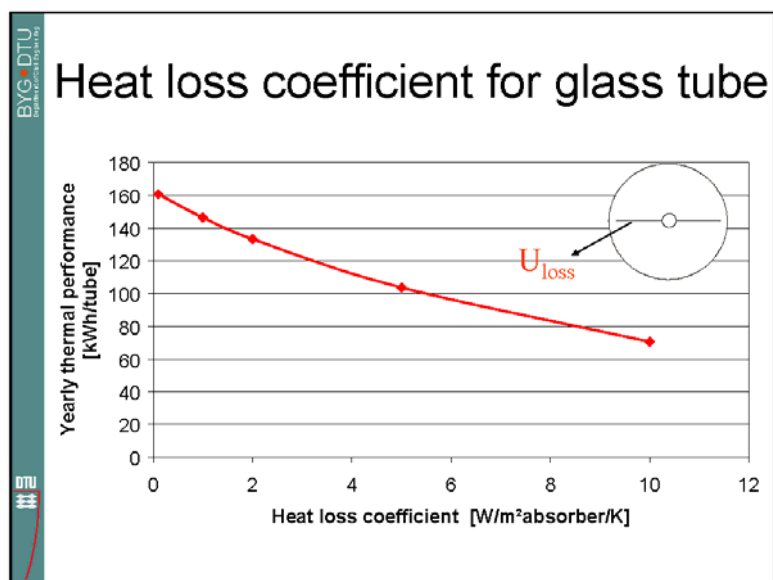
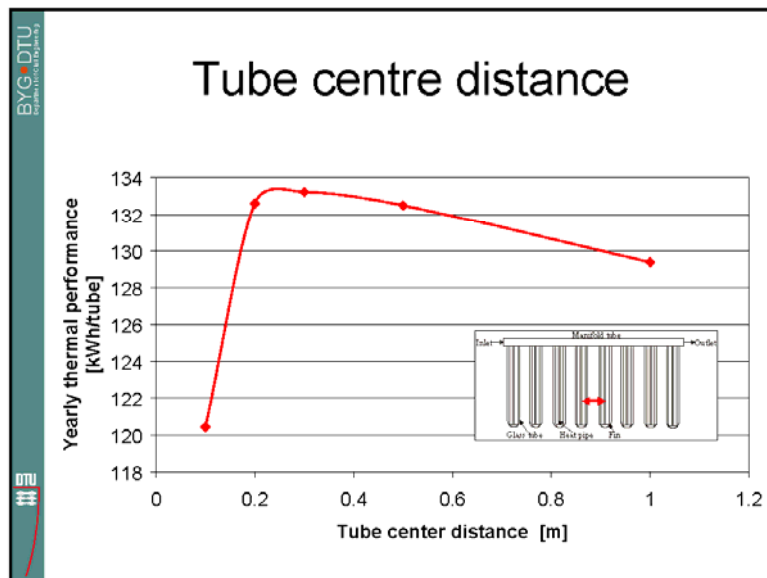


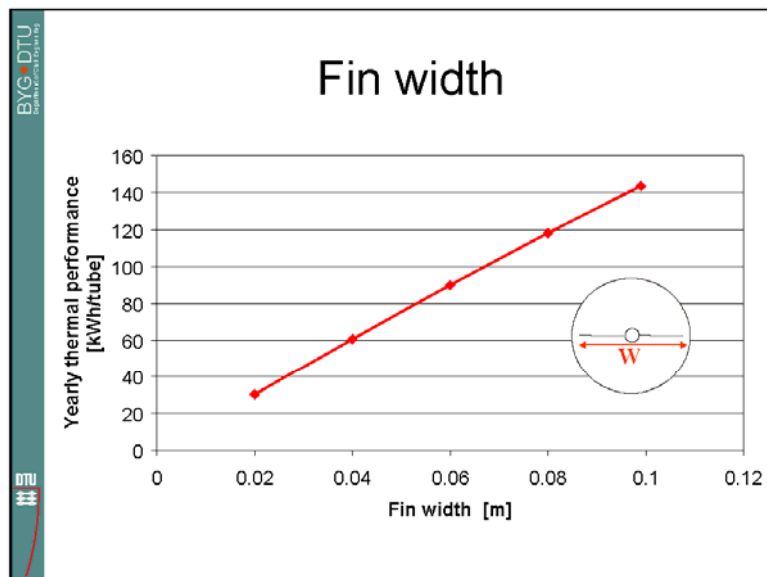
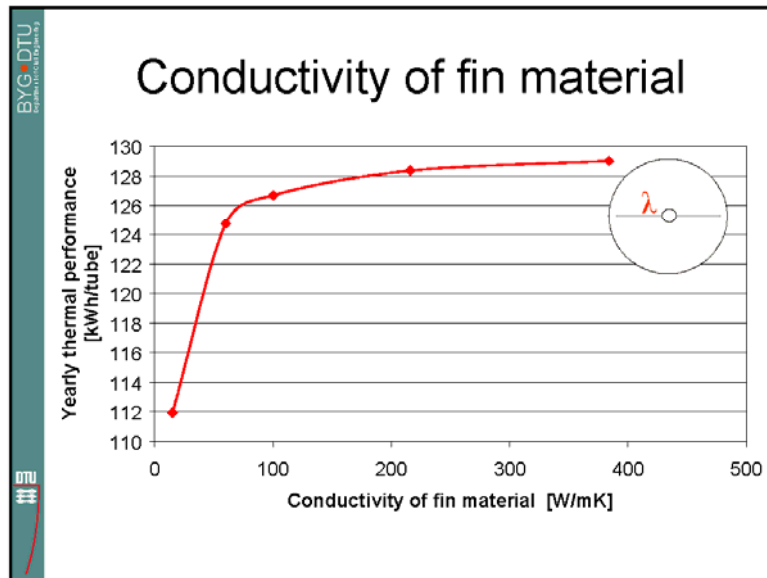
BYG-DTU
Department of Building Physics

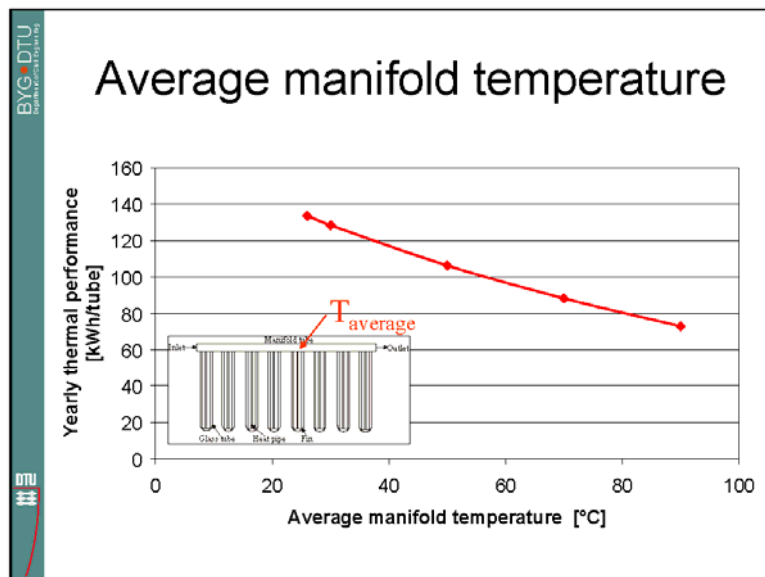
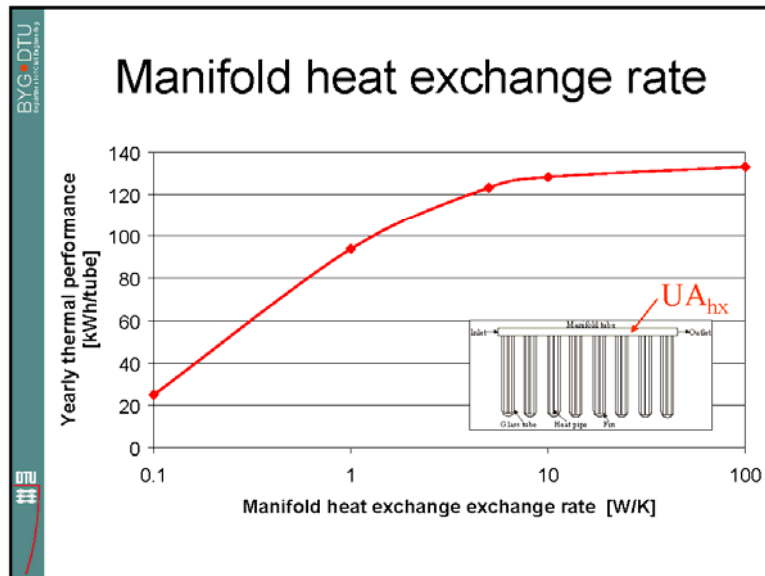
Calculation examples

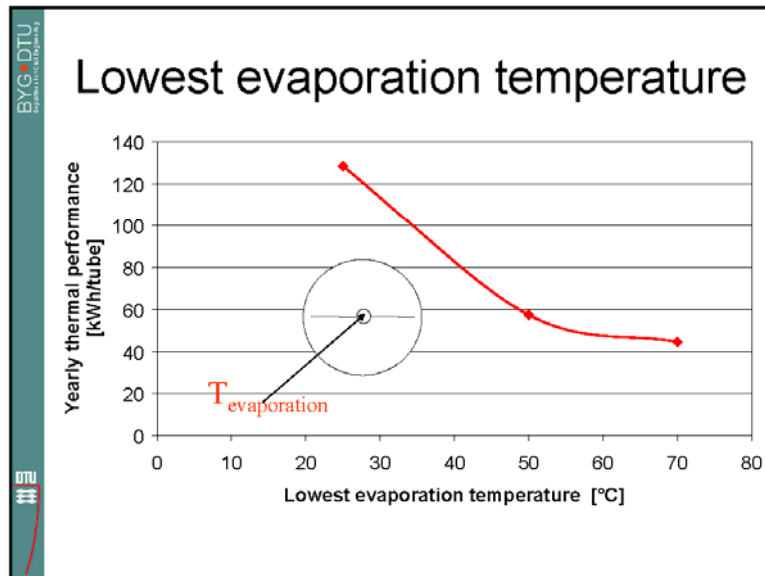
- Copenhagen weather data
- Simulation of yearly thermal performance
- Glass tube diameter = 0.1 m
- Collector operating temperature = 30°C
- Lowest evaporation temperature = 25°C
- Flat fin heat pipe evacuated tubular collector

The diagram shows a cross-section of a flat fin heat pipe evacuated tubular collector. The diameter is $d=0.1$ m, the width is $w=0.085$ m, and the wall thickness is $\delta=0.0002$ m.









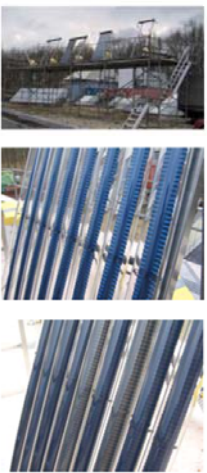
Preliminary conclusions from theoretical work

- Developed two new Trnsys collector types for heat pipes with double sided absorbers
- Detailed view factor modelling
- Detailed shadow modelling
- Detailed fin temperature modelling
- Model input = Exact collector design
- Detailed optimization of collector design is now possible

BYG-DTU
Department of Building Research
DTU

Further work

- Measurements
- Final validation of theoretical models
- Parameter studies
 - Absorber materials
 - Collector design
- Cost performance analyses



BYG-DTU
Department of Building Research
DTU

Thank you for your attention



Photo aspect ratio not correct